The Plant Cell, Vol. 32: 1136–1160, April 2020, www.plantcell.org © 2020 ASPB.

Kalanchoë PPC1 Is Essential for Crassulacean Acid Metabolism and the Regulation of Core Circadian Clock and Guard Cell Signaling Genes[CC-BY]

Susanna F. Boxall, Nirja Kadu, Louisa V. Dever, Jana Kneřová, Jade L. Waller, Peter J. D. Gould, and James Hartwell[1]

Department of Functional and Comparative Genomics, Institute of Integrative Biology, University of Liverpool, Liverpool L69 7ZB, United Kingdom

ORCID IDs: 0000-0002-8753-101X (S.F.B.); 0000-0002-2557-3791 (N.K.); 0000-0001-7801-5622 (L.V.D.); 0000-0002-9562-4339 (J.K.); 0000-0002-0922-4284 (J.L.W.); 0000-0002-0709-1190 (P.J.D.G.); 0000-0001-5000-223X (J.H.)

Unlike C_3 plants, Crassulacean acid metabolism (CAM) plants fix CO_2 in the dark using phospho*enol*pyruvate carboxylase (PPC; EC 4.1.1.31). PPC combines phospho*enol*pyruvate with CO_2 (as HCO_3^-), forming oxaloacetate. The oxaloacetate is converted to malate, leading to malic acid accumulation in the vacuole, which peaks at dawn. During the light period, malate decarboxylation concentrates CO_2 around Rubisco for secondary fixation. CAM mutants lacking PPC have not been described. Here, we employed RNA interference to silence the CAM isogene *PPC1* in *Kalanchoë laxiflora*. Line *rPPC1-B* lacked *PPC1* transcripts, PPC activity, dark period CO_2 fixation, and nocturnal malate accumulation. Light period stomatal closure was also perturbed, and the plants displayed reduced but detectable dark period stomatal conductance and arrhythmia of the CAM CO_2 fixation circadian rhythm under constant light and temperature free-running conditions. By contrast, the rhythm of delayed fluorescence was enhanced in plants lacking *PPC1*. Furthermore, a subset of gene transcripts within the central circadian oscillator was upregulated and oscillated robustly in this line. The regulation of guard cell genes involved in controlling stomatal movements was also perturbed in *rPPC1-B*. These findings provide direct evidence that the regulatory patterns of key guard cell signaling genes are linked with the characteristic inverse pattern of stomatal opening and closing during CAM.

INTRODUCTION

Crassulacean acid metabolism (CAM) is a pathway of photosynthetic CO_2 fixation found in species adapted to low rainfall and/or periodic drought, such as the Madagascan-endemic succulent *Kalanchoë laxiflora* (family: Crassulaceae; order: Saxifragales; Hartwell et al., 2016). CAM species open their stomata for primary atmospheric CO_2 fixation in the dark, when their environment is cooler and more humid, and close their stomata in the light, when the atmosphere is at its hottest and driest (Osmond, 1978). The increased water use efficiency (WUE) and CO_2 fixation efficiency of CAM species have led to the proposal that the use of productive CAM crop species, including certain *Agave* and *Opuntia* species, represents a viable approach to generating biomass for biofuels and renewable platform chemicals for industry through their cultivation on seasonally dry lands that are not well suited to food crop production (Borland et al., 2009; Cushman et al., 2015). Furthermore, efforts are underway to engineer CAM into key C_3 crops (Borland et al., 2014, 2015; DePaoli et al., 2014; Lim et al., 2019).

Recently, genome, transcriptome, proteome, and metabolome data sets for a phylogenetically diverse range of CAM plants of independent origin have started to open up a large catalog of putative CAM genes. CAM species represented by published omics data sets span orchids (*Phalaenopsis equestris* and *Erycina pusilla*, Orchidaceae, monocots), pineapple (*Ananas comosus*, Bromeliaceae, monocots), *Agave* (*A. americana*, *A. deserti*, *A. tequilana*, Agavaceae, monocots), *Yucca* (*Y. aloifolia*, Asparagaceae, monocots), *Kalanchoë* (*K. fedtschenkoi* and *K. laxiflora*, Crassulaceae, eudicots), *Mesembryanthemum* (*M. crystallinum*, Aizoaceae, eudicots), and waterleaf (*Talinum triangulare*, Portulacaceae, eudicots; Cushman et al., 2008; Gross et al., 2013; Cai et al., 2015; Ming et al., 2015; Abraham et al., 2016; Brilhaus et al., 2016; Hartwell et al., 2016; Yang et al., 2017; Heyduk et al., 2018, 2019). The optimal exploitation of CAM will be facilitated through decoding the molecular-genetic blueprint for CAM from these genomes and transcriptomes. In turn, to be fully realized, this opportunity requires functional genomics approaches using transgenic and/or mutant lines of model CAM species to test and define in detail candidate CAM gene functions (Dever et al., 2015; Hartwell et al., 2016; Boxall et al., 2017).

During CAM, primary nocturnal CO_2 assimilation is catalyzed by phospho*enol*pyruvate (PEP) carboxylase (PPC), generating oxaloacetate, which is rapidly converted to malate and stored in the vacuole as malic acid (Borland et al., 2009). At dawn, malic acid is transported out of the vacuole and malate is decarboxylated in the mitochondria, chloroplasts, and/or cytosol, and the released CO_2 is refixed by Rubisco behind closed stomata (Borland et al., 2009).

[1] Address correspondence to james.hartwell@liverpool.ac.uk.
The author responsible for distribution of materials integral to the findings presented in this article in accordance with the policy described in the Instructions for Authors (www.plantcell.org) is: James Hartwell (james.hartwell@liverpool.ac.uk).

www.plantcell.org/cgi/doi/10.1105/tpc.19.00481

IN A NUTSHELL

Background: Severe droughts and high temperatures are becoming more frequent due to climate change, making it increasingly challenging to grow crops productively in many major agricultural regions worldwide. Scientists are therefore exploring new ways to enhance the ability of crop species to conserve precious water. One potential solution relates to a water-wise version of photosynthesis known as Crassulacean acid metabolism (CAM). CAM plants capture CO_2 from the atmosphere at night, when the air is cooler and holds more moisture. This means that they only need to open their leaf or stem pores at night, so they don't lose as much water as all of the other plants that open their pores in the heat of the day.

Question: To capture CO_2 when it's dark, CAM plants use an enzyme called phosphenolpyruvate carboxylase (PPC). We set out to discover what happens to the Madagascan CAM plant *Kalanchoë laxiflora* (Milky Widow's Thrill) when it is no longer able to use PPC to capture CO_2 at night.

Findings: We discovered that Kalanchoë went back to using the original form of photosynthesis used by most plants (known as C_3) when it didn't have PPC1. CO_2 was captured from the air during the hot, dry day, and so the leaves lost more water. Importantly, these *PPC1*-silenced plants didn't perform as well as fully functional Kalanchoës during drought stress. This allowed us to quantify the advantage that Kalanchoë has gained by evolving CAM photosynthesis. We also discovered that other key aspects of Kalanchoë's biology changed without PPC1 working the night shift. In particular, the functioning of genes that keep time in the plant's internal clock, and several involved in opening and closing of the leaf pores, changed in ways that open up new questions for future research.

Next steps: Our discoveries define how much PPC we need to switch on in a C_3 crop like soybean so that it can use CAM and save water. In addition, further work in Kalanchoë will allow us to explore the functions of the other genes whose expression changed when *PPC1* was switched off.

Strict temporal control prevents a futile cycle between the enzymes and metabolite transporters driving malate production in the dark and those driving malate decarboxylation in the light (Hartwell, 2006). PPC regulation is central to this temporal control. PPC is activated allosterically by glucose 6-phosphate (G6P) and inhibited by malate, Asp, and Glu (O'Leary et al., 2011). The circadian clock optimizes the timing of the CAM carboxylation and decarboxylation pathways to prevent futile cycling (Wilkins, 1992; Hartwell, 2005).

Temporal optimization of PPC involves protein phosphorylation in the dark period, a process catalyzed by the circadian clock-controlled protein kinase, phospho*enol*pyruvate carboxylase kinase (PPCK; Carter et al., 1991; Hartwell et al., 1996, 1999; Taybi et al., 2000; Boxall et al., 2005). Phosphorylated PPC is less sensitive to feedback inhibition by malate, which in turn ensures sustained CO_2 fixation as malic acid accumulates throughout the dark period (Nimmo et al., 1984; Carter et al., 1991; Boxall et al., 2017). In the light, PPC becomes more sensitive to inhibition by malate due to dephosphorylation by a protein phosphatase type 2A (PP2A), which is not known to be subject to circadian control (Carter et al., 1990).

In CAM species such as *Kalanchoë*, the PEP substrate required for nocturnal atmospheric CO_2 fixation by PPC is generated through starch breakdown and glycolysis (Borland et al., 2016). In the C_3 model species Arabidopsis (*Arabidopsis thaliana*), nocturnal degradation of leaf starch begins with the phosphorylation of glucan chains by GLUCAN WATER DIKINASE (GWD) and PHOSPHOGLUCAN WATER DIKINASE (Ritte et al., 2006). The phosphorylated glucan chains are then further degraded by ALPHA-AMYLASES (AMYs) and BETA-AMYLASES (BAMs) to maltose and glucose. Nocturnal starch hydrolysis by BAMs is the predominant pathway in C_3 leaves, with chloroplastic BAM3 being the major BAM isozyme driving nocturnal starch degradation in photosynthetic leaf mesophyll cells of Arabidopsis (Fulton et al., 2008). BAM1, BAM2, and BAM5 to BAM9 are not required for nocturnal starch degradation in Arabidopsis leaf mesophyll cells (Santelia and Lunn, 2017). Maltose and glucose are exported from chloroplasts by MALTOSE EXCESS1 (MEX1) and PLASTIDIC GLUCOSE TRANSPORTER (pGlcT), respectively, with MEX1 being the predominant C_3 route for carbon export (Smith et al., 2005). In the facultative CAM species *M. crystallinum*, chloroplasts possess transporters for triose phosphate (TPT), G6P (GPT), glucose (pGlcT) and maltose (MEX1; Neuhaus and Schulte, 1996; Kore-eda et al., 2005, 2013). Chloroplasts from C_3 leaves of *M. crystallinum* exported maltose during starch degradation, whereas chloroplasts isolated from CAM-induced leaves predominantly exported G6P, supporting the proposal that starch is broken down via plastidic starch phosphorylase (PHS1) during nocturnal CO_2 fixation (Neuhaus and Schulte, 1996).

A further defining characteristic of CAM relates to nocturnal stomatal opening and CO_2 uptake as well as light period stomatal closure during malate decarboxylation and peak internal CO_2 supply (Males and Griffiths, 2017). Stomatal control in CAM species is the inverse of the stomatal regulation observed in C_3 species (Borland et al., 2014). The opening and closing of stomata are driven by the turgor of the guard cell (GC) pair that surrounds the stomatal pore. High turgor drives stomatal opening, and a reduction in turgor leads to stomatal closure. The increase in turgor during opening is driven by the accumulation of K^+, Cl^-, and malate^{2-} ions plus sugars in the GCs (Jezek and Blatt, 2017). The closure of stomata is driven by a reversal of GC ion channels and metabolism, with K^+ and Cl^- being transported out, and metabolites being turned over within the GCs. Stomatal aperture responds to changing light, CO_2, abscisic acid (ABA), solutes, and water availability (Kim et al., 2010; Daloso et al., 2016; Horrer et al., 2016; Zhang et al., 2018; Yoshida et al., 2019).

In addition to its role in CAM and C_4 plants, PPC performs an anapleurotic function by replenishing tricarboxylic acid cycle

intermediates utilized for amino acid biosynthesis (Chollet et al., 1996). PPC also functions in the formation of malate as a counter anion for light period opening in C_3 GCs and supports nitrogen fixation into amino acids in legume root nodules (Chollet et al., 1996). The major leaf PPCs in Arabidopsis, which are encoded by *PPC1* (AT1G53310) and *PPC2* (AT2G42600), are crucial for leaf carbon and nitrogen metabolism (Shi et al., 2015). Compared with the wild type, the double *ppc1 ppc2* null mutant accumulates less starch and sucrose and has reduced malate, citrate, and ammonium assimilation; these metabolic changes lead to a severe, growth-arrested phenotype (Shi et al., 2015).

Although PPC catalyzes primary CO_2 fixation in CAM and C_4 plants, the only reported PPC mutants are for the C_4 eudicot grain amaranth (*Amaranthus edulis*) and the C_4 monocot green foxtail (*Setaria viridis*; Dever et al., 1995; Alonso-Cantabrana et al., 2018). C_4 PPC catalyzes light period primary CO_2 fixation in mesophyll cells, generating malate or Asp, which is shuttled to bundle sheath cells for decarboxylation (von Caemmerer and Furbank, 2003). This leads to the concentration of CO_2 around Rubisco, which is only present in bundle sheath cells. Photorespiration is thus minimized. The loss of the C_4 *PPC* isogene in *A. edulis* caused a severe and lethal growth phenotype in normal air, with the homozygous mutant plants only managing to reach flowering and set seed when grown at highly elevated CO_2 (Dever et al., 1995). In *S. viridis*, the C_4 *PPC* expression was reduced to very low levels using RNA interference (RNAi) in transgenic lines (Alonso-Cantabrana et al., 2018). These lines grew very slowly even at 2% CO_2 (normal air is 0.04%) and developed increased numbers of plasmodesmatal pit fields at the mesophyll-bundle sheath interface (Alonso-Cantabrana et al., 2018). By contrast, no CAM mutants lacking PPC have been described, but transgenic lines of *Kalanchoë* lacking the light period, decarboxylation pathway enzymes mitochondrial NAD-malic enzyme (NAD-ME) and pyruvate orthophosphate dikinase (PPDK) displayed a nearly complete loss of dark CO_2 fixation and failed to turn over significant malate during the light period (Dever et al., 2015). In *Kalanchoë*, NAD-ME catalyzes the conversion of malate to pyruvate and CO_2 during the light period, and PPDK converts the pyruvate to PEP, allowing subsequent recycling of the by-product of malate decarboxylation through gluconeogenesis to stored starch (Dever et al., 2015). Another CAM mutant lacking the starch synthesis pathway enzyme plastidic phosphoglucomutase has been reported in the inducible CAM species *M. crystallinum* (Cushman et al., 2008).

In addition, the CAM-associated *PPCK1* gene in *Kalanchoë* was silenced using RNAi, which not only led to a reduction in dark period CO_2 fixation but also perturbed the operation of the central circadian clock (Boxall et al., 2017). However, even the strongest *PPCK1* RNAi line was still able to achieve ~33% of the dark period CO_2 fixation observed in the wild type (Boxall et al., 2017). These findings led us here to develop transgenic *K. laxiflora* lines in which the CAM-associated isogene of *PPC* itself (isogene *PPC1*) was downregulated using RNAi. The most strongly silenced line, *rPPC1-B*, lacked *PPC1* transcripts and activity, and this resulted in the complete loss of dark CO_2 fixation associated with CAM and arrhythmia of the CAM CO_2 fixation rhythm under constant light and temperature (LL) free-running conditions. Growth of *rPPC1-B* plants was reduced relative to the wild type under both well-watered and drought-stressed conditions. The plants reverted to fixing CO_2 in the light, especially in their youngest leaf pairs. Although the circadian rhythm of CO_2 fixation dampened rapidly toward arrhythmia in the *rPPC1-B* line, the distinct circadian clock output of delayed fluorescence (DF) as well as the oscillations of the transcript abundances of a subset of core circadian clock genes were enhanced. Furthermore, the temporal phasing of a wide range of GC-specific signaling genes involved in opening and closing was perturbed relative to the wild type in *rPPC1-B*. These findings shed light on important regulators underpinning the inverse stomatal control associated with CAM.

RESULTS

Initial Screening and Characterization of *PPC1* RNAi Lines of *K. laxiflora*

As *K. laxiflora* is relatively slow-growing, with flowering and seed set taking ~9 months seed-to-seed (Hartwell et al., 2016), data are presented for independent primary transformants that were propagated clonally via leaf margin plantlets and/or stem cuttings. We initially screened primary transformants using high-throughput leaf disc tests for starch and acidity at dawn and dusk (Cushman et al., 2008; Dever et al., 2015). We screened independent transgenic lines that acidified less during the dark period than the wild type for the steady state abundance of *PPC1* transcripts using RT-qPCR (Figure 1). Line *rPPC1-B* displayed a complete loss of *PPC1* transcripts, whereas *rPPC1-A* had an intermediate level of *PPC1* transcripts (Figure 1A). The other plant-type *PPC* genes (*PPC2*, *PPC3*, and *PPC4*) were upregulated relative to the wild type, with their peak phased to dawn (Figures 1B to 1D). *PPC2* was upregulated in line *rPPC1-B* at 6 and 10 h into the 12-h dark period (Figure 1B).

In line *rPPC1-B*, *PPCK1*, encoding the protein kinase that phosphorylates the CAM-associated protein PPC1, was downregulated during its dark period phased peak and appeared to be slightly upregulated at 2 h after dawn (Figure 1E). The other two detectable *PPCK* genes, *PPCK2* and *PPCK3*, were upregulated in *rPPC1-B*, with *PPCK2* induced fivefold when it reached its 24-h peak in the middle of the dark period, 4 h after the wild-type peak (Figure 1F). *PPCK3* peaked in the middle of the light period, when it reached a level almost eightfold greater than the wild type (Figure 1G).

Loss of *PPC1* Transcripts Leads to Loss of PPC Protein and Activity

Immunoblotting using an antibody raised against purified CAM-specific PPC protein from *K. fedtschenkoi* leaves (Nimmo et al., 1986; Figure 2) revealed reduced levels of PPC protein in *rPPC1-A* and no detectable PPC in *rPPC1-B* (Figure 2A).

We also measured the level of phospho-PPC using immunoblotting (Figure 2B). Phospho-PPC levels were lower in *rPPC1-A* than the wild type, while *rPPC1-B* lacked detectable phospho-PPC (Figure 2B), which was consistent with the level of PPC (Figure 2A). Although *PPC2* was upregulated in *rPPC1-B* (Figure 1B), it was not detected at the protein level by the PPC antibody (Figure 2A).

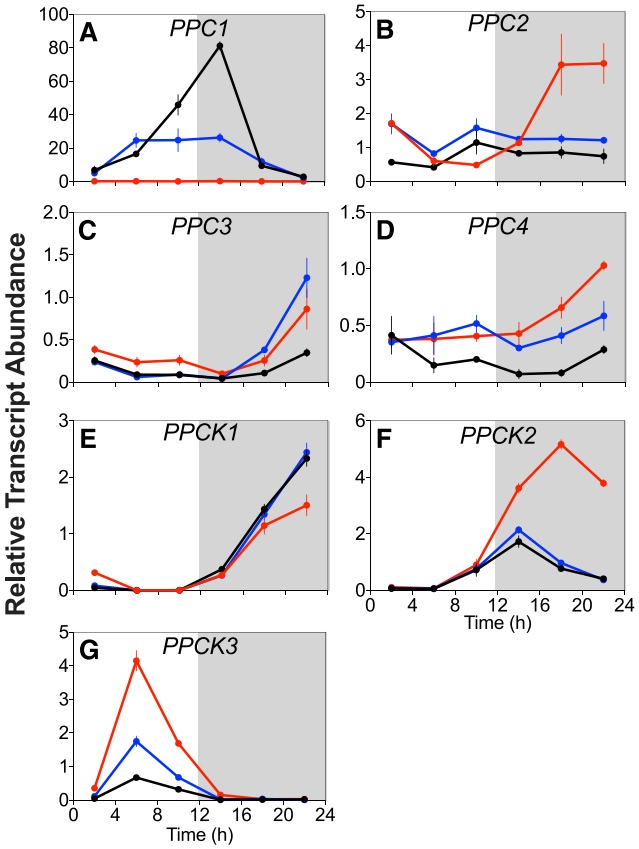

Figure 1. Confirmation of Target Gene Silencing in Transgenic *K. laxiflora* RNAi Lines *rPPC1-A* and *rPPC1-B*.

Gene transcript abundance in leaf pair 6 (LP6) was measured using RT-qPCR for target genes *PPC1* **(A)**, *PPC2* **(B)**, *PPC3* **(C)**, *PPC4* **(D)**, *PPCK1* **(E)**, *PPCK2* **(F)**, and *PPCK3* **(G)**. LP6 were sampled every 4 h across the 12-h-light/12-h-dark cycle. A thioesterase/thiol ester dehydrase-isomerase superfamily gene (*TEDI*) was amplified from the same cDNAs as a reference gene. Gene transcript abundance data represent means of three technical replicates for biological triplicates and were normalized to the loading control gene (*TEDI*); error bars represent the SE. In all cases, plants were entrained under 12-h-light/12-h-dark cycles for 7 d prior to sampling. Black data are for the wild type, blue data for *rPPC1-A*, and red data for *rPPC1-B*.

Furthermore, despite *PPCK2* and *PPCK3* being upregulated by fivefold to eightfold in *rPPC1-B* (Figures 1F and 1G), any protein produced from these transcripts did not phosphorylate any PPC2 protein that may have resulted from the induced *PPC2* transcripts (Figure 2B), at least not within the limits of detection with this immunoblotting technique. We used rapidly desalted leaf extracts to measure the apparent inhibitor constant (K_i) of PPC for L-malate. The K_i was higher in the dark than in the light for the wild type and *rPPC1-A*, but no change in the K_i was detected for *rPPC1-B* (Supplemental Figure 1). Furthermore, PPC activity was not detected in rapidly desalted extracts from *rPPC1-B* leaves, whereas *rPPC1-A* displayed reduced but detectable PPC activity, at 43% of the wild-type level (Figure 2C; Supplemental Table 1).

PPDK, which functions in concert with NAD-ME during the light period as part of the CAM malate decarboxylation pathway (Dever et al., 2015), was measured on immunoblots using specific antibodies against PPDK and phospho-PPDK (Chastain et al., 2000, 2002). The blots showed a similar amount of PPDK protein over the diel cycle in the wild type, *rPPC1-A*, and *rPPC1-B* (Figure 2D), confirming the even protein loading of the blots, which was further supported by the images of Coomassie blue-stained gels (Supplemental Figure 1). In *Kalanchoë*, PPDK is inactivated in the dark by phosphorylation by PPDK-regulatory protein (PPDK-RP), which also activates PPDK in the light through dephosphorylation (Dever et al., 2015). In the wild type,

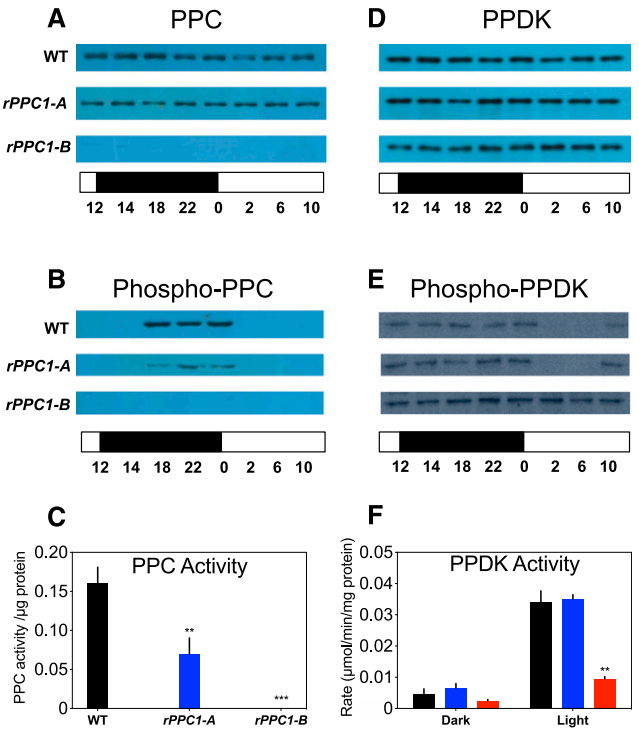

Figure 2. Loss of *PPC1* Transcripts Leads to Loss of PPC Protein and Activity and Failure to Activate PPDK in the Light.

(A) and **(B)** Total leaf protein from leaf pair 6 (LP6) was isolated from leaves sampled at dawn and dusk plus every 4 h, starting at 2 h into the light period, across the 12-h-light/12-h-dark cycle, separated using SDS-PAGE, and used for immunoblot analyses with antibodies raised to PPC **(A)** and phospho-PPC **(B)**.

(C) PPC activity was measured in rapidly desalted extracts from LP6. **, *rPPC1-A*, P = 0.0054; ***, *rPPC1-B*, P = 0.00016.

(D) Anti-PPDK immunoblot.

(E) Anti-phospho-PPDK immunoblot.

(F) PPDK activity was measured in leaf extracts prepared from both dark leaves and illuminated leaves. **, *rPPC1-B*, P = 0.003.

The activities of PPC, measured 6 h into the light period, and PPDK, measured at both 6 h into the dark period and 6 h into the light period, were means of three technical replicates of three biological replicates, and error bars represent the SE. The white bars below panels **(A)**, **(B)**, **(D)**, and **(E)** represent the 12-h-light period, and the black bars represent the 12-h-dark period. In panels **(C)** and **(F)**, black data are for the wild type, blue data for *rPPC1-A*, and red data for *rPPC1-B*. Asterisks indicate significant differences from the wild type based on Student's *t* test. All Student's *t* test parameters are presented in Supplemental Tables 1 and 2.

immunoblotting of phospho-PPDK revealed that PPDK was dephosphorylated, and therefore likely to be fully active, between 02:00 and 06:00 h in the light when it is required for the conversion of pyruvate, from malate decarboxylation, to PEP, thereby facilitating the recycling of carbon through gluconeogenesis to starch (Figure 2E). Line *rPPC1-A* showed the same pattern of PPDK phosphorylation/dephosphorylation as the wild type (Figure 2E). However, PPDK was phosphorylated throughout the 24-h cycle in *rPPC1-B* (Figure 2E) and was therefore likely to be inactive. Consistent with this prediction, loss of the light period dephosphorylation of PPDK in *rPPC1-B* correlated with a significant decrease in PPDK activity in the light, whereas the wild type and line *rPPC1-A* showed strongly light-induced levels of PPDK activity that correlated with the detected level of PPDK dephosphorylation in the light (Figure 2F; Supplemental Table 2).

Malate, Starch, and Soluble Sugar Levels

During CAM in *Kalanchoë*, primary nocturnal fixation of atmospheric CO_2 (as HCO_3^-) results in vacuolar malic acid accumulation throughout the dark period. Starch accumulates during the light period and is broken down during the dark period to provide PEP as the substrate for carboxylation by PPC. Starch is also broken down in a rapid burst at dawn to form soluble sugars (Wild et al., 2010; Boxall et al., 2017). As the lack of CAM-associated *PPC1* was predicted to prevent primary nocturnal carboxylation, we measured metabolites including malate, starch, and soluble sugars every 4 h over the 24-h cycle (Figure 3).

Wild-type plants accumulated 130 μmol g^{-1} fresh weight malate by dawn, whereas *rPPC1-A* and *rPPC1-B* accumulated 75 and 19.5 μmol g^{-1} fresh weight, respectively (Figure 3A). The Δ-malate values for the wild type, *rPPC1-A*, and *rPPC1-B* were 124.0, 64.3, and 16.2 μmol g^{-1} fresh weight, respectively (Figure 3A). During the diel cycle, *rPPC1-A* and *rPPC1-B* synthesized 100 and 41% of the amount of starch accumulated by the wild type, respectively (Figure 3B). The Δ-starch values for the wild type, *rPPC1-A*, and *rPPC1-B* were 8.5, 8.5, and 3.5 mg starch g^{-1} fresh weight (Figure 3B). Lines *rPPC1-A* and *rPPC1-B* accumulated 51 and 15% of the amount of sucrose accumulated by the wild type (Figure 3C) and 83 and 69% of the level of glucose, respectively (Figure 3D). Glucose accumulated 4 h after the sucrose peak in the wild type, whereas glucose levels peaked at the same time as sucrose in lines *rPPC1-A* and *rPPC1-B* (Figures 3C and 3D). Finally, lines *rPPC1-A* and *rPPC1-B* accumulated 113 and 61% of the amount of fructose, respectively, compared with the wild type (Figure 3E). In *rPPC1-B*, the daily maxima for fructose and glucose coincided with that of sucrose at 2 h after dawn (Figures 3C to 3E). While no direct evidence was obtained to explain these shifts in the timing of the sucrose, glucose, and fructose daily maxima, the most straightforward explanation is that the observed changes in the timing of photosynthetic CO_2 fixation and starch accumulation and turnover in the *rPPC1-B* transgenic line resulted in the observed changes in the timing of the soluble sugar peaks.

Growth Analysis in Well-Watered Versus Drought-Stressed Conditions

CAM is widely regarded as an adaptation to drought, and so it was important to compare the growth performance of the wild type (full CAM) with that of *rPPC1-A* (small reduction in CAM) and *rPPC1-B* (no CAM) plants under both well-watered and drought-stressed conditions (Figure 3F; Supplemental Figure 2; Supplemental Data Set 1). *rPPC1-B* plants were significantly smaller than wild-type plants in both well-watered and drought-stressed conditions (Figure 3F; Supplemental Figure 2). In well-watered conditions, the shoot dry weight of *rPPC1-B* was 21% less than that of the wild type (Figure 3F), but the shoot dry weight of *rPPC1-A* was not significantly different from that of the wild type. Under drought-stressed conditions, the shoot dry weight of line *rPPC1-B* was 12% lower than that of the wild type (Figure 3F). A visual inspection of representative 4-month-old plants demonstrated that *rPPC1-B* was smaller than the wild type and *rPPC1-A* (Figure 3G), which is consistent with the shoot dry weight data (Figure 3F). Shoot fresh weight was also significantly reduced in well-watered and drought-stressed *rPPC1-B*, whereas the only significant difference in belowground root tissues was for *rPPC1-B* under drought stress, which displayed an increase in root fresh weight that was only just significant ($P = 0.0483$; Supplemental Figure 2). Furthermore, *rPPC1-B* displayed a reduced degree of leaf in-rolling in response to drought relative to the wild type (Supplemental Figure 3), even though it lost just as much water during drought as the wild type (Supplemental Figure 2).

Gas-Exchange Characteristics under Light/Dark Cycles

We measured gas exchange in mature CAM leaves (leaf pair 6 [LP6]) of each line over a 12-h-light, 25°C, 60% humidity/12-h-dark, 15°C, 70% humidity cycle using an infrared gas analyzer (LI-COR LI-6400XT; Figures 4A to 4C). Over the 24-h diel cycle, the wild type fixed 297 μmol CO_2 m^{-2}, *rPPC1-A* fixed 320 μmol CO_2 m^{-2}, and *rPPC1-B* fixed 230 μmol CO_2 m^{-2} (Figure 4A). Net CO_2 fixation was 23% less than in the wild type in line *rPPC1-B*, whereas it was 15% greater in line *rPPC1-A* (Figure 4A).

The four phases of CAM (Osmond, 1978) are indicated on the CO_2 exchange graph in Figure 4A. Phase I corresponds to the period of nocturnal atmospheric CO_2 fixation to vacuolar malic acid in the wild type, and phases II, III, and IV define the peaks and troughs of CO_2 fixation and stomatal conductance across the 12-h-light period (Figures 4A and 4B). Specifically, phase II refers to the sharp peak of CO_2 fixation in the 1 to 2 h after dawn, phase III defines the period of refixation of CO_2 from malate decarboxylation by Rubisco behind closed stomata that spans the middle of the light period, and phase IV occurs in younger leaves of well-watered plants and corresponds to the period in the late afternoon when stomata reopen and atmospheric CO_2 is fixed directly by Rubisco (Osmond, 1978). Note that the data in blue for *rPPC1-A* provide the best example of this four-phase framework for CAM CO_2 fixation and stomatal physiology (Figure 4A). By contrast, LP6 of the wild type performed full CAM defined by phase I in the dark and phase III in the light (Figure 4A). By calculating the total area under or over the CO_2-exchange curves in Figure 4A, and calculating these areas separately for the 12-h-light and 12-h-dark periods, it was possible to quantify the amounts of CO_2 fixed by each line during either the light period or the dark period. In the light period (phases II through IV), wild-type leaves fixed negligible amounts of atmospheric CO_2, whereas *rPPC1-B* fixed a total of 265 μmol m^{-2} and *rPPC1-A* fixed 89 μmol m^{-2} (Figure 4A). In the dark period (phase I), the wild type fixed 297 μmol CO_2 m^{-2} and

rPPC1-A fixed 226 μmol CO_2 m^{-2}, but *rPPC1-B* respired 35 μmol CO_2 m^{-2} (Figure 4A). The loss of nocturnal CO_2 fixation in *rPPC1-B* (Figure 4A) corresponded with the lack of the CAM-associated *PPC1* (Figures 1 and 2). LP6 of *rPPC1-A* fixed 24% less nocturnal CO_2 than the wild type, but, in contrast to the wild type, it continued some light period CO_2 capture (Figure 4A).

Apart from opening briefly for phase II, just after lights-on, the attached LP6 of the wild type closed its stomata in the light and opened them throughout the dark, when stomatal conductance tracked CO_2 uptake (Figure 4B). In *rPPC1-B*, stomata stayed open in the light, closed briefly at dusk, and opened slightly throughout the dark, with a small peak prior to dawn (Figure 4B).

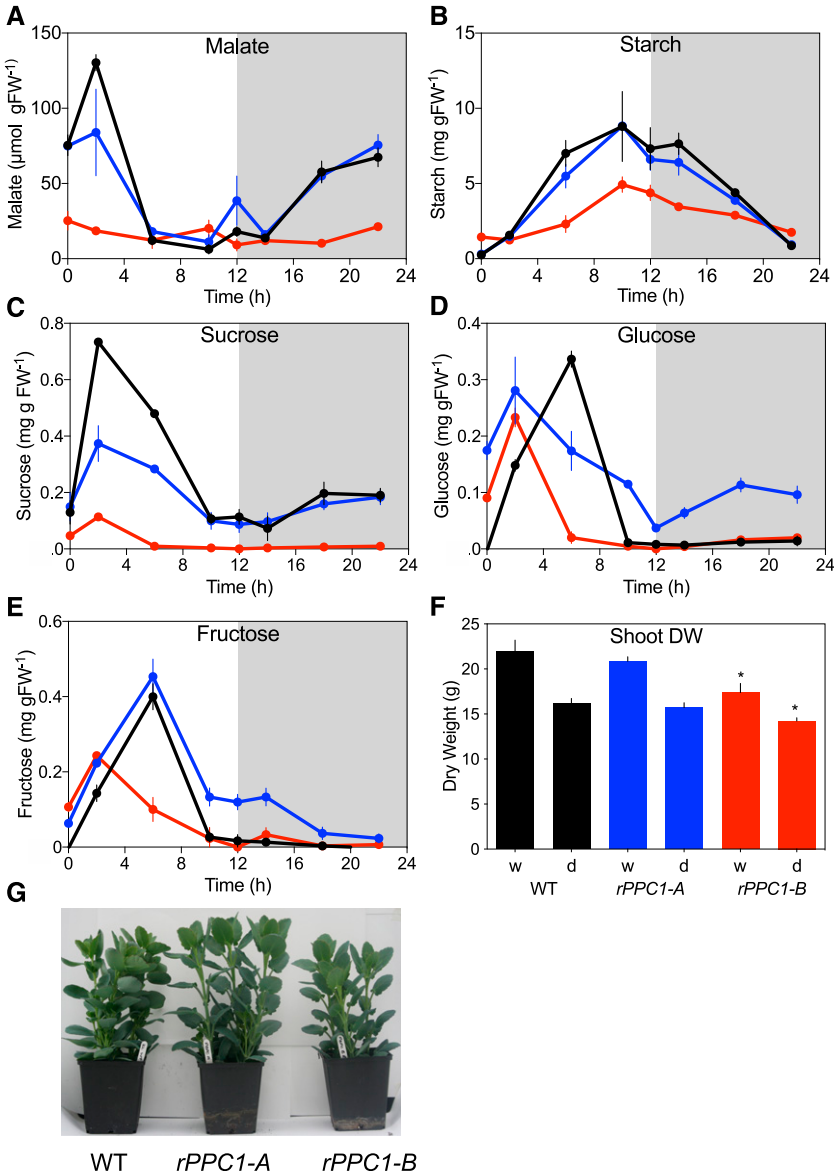

Figure 3. Impact of Silencing *PPC1* on Malate, Starch, Soluble Sugars, and Growth.

(A) to **(E)** The contents of malate **(A)**, starch **(B)**, sucrose **(C)**, glucose **(D)**, and fructose **(E)** were determined from leaf pair 6 (LP6) samples collected every 4 h using plants entrained under 12-h-light/12-h-dark cycles. Methanol extracts were prepared from the leaves from the wild type, *rPPC1-A*, and *rPPC1-B* and used for malate and soluble sugar determination, whereas starch was measured in the insoluble pellet. FW, fresh weight.

(F) Dry weight (DW) of 148-d-old greenhouse-grown plants, either well-watered (w) or drought-stressed for the last 28 d (d). Asterisks denote significant differences between the wild type and *rPPC1-B* based on Student's *t* test. Well-watered *rPPC1-B*, *, $P = 0.017$; drought-stressed *rPPC1-B*, *, $P = 0.011$; $n =$ 6 to 9 developmentally synchronized, clonal plants per line. See Supplemental Data Set 1 for full parameters from Student's *t* test results for the relative growth data.

(G) Four-month-old plants raised in a greenhouse under 16-h-light/8-h-dark cycles.

In all graphs, black data are for the wild type, blue data for *rPPC1-A*, and red data for *rPPC1-B*. Error bars represent the SE.

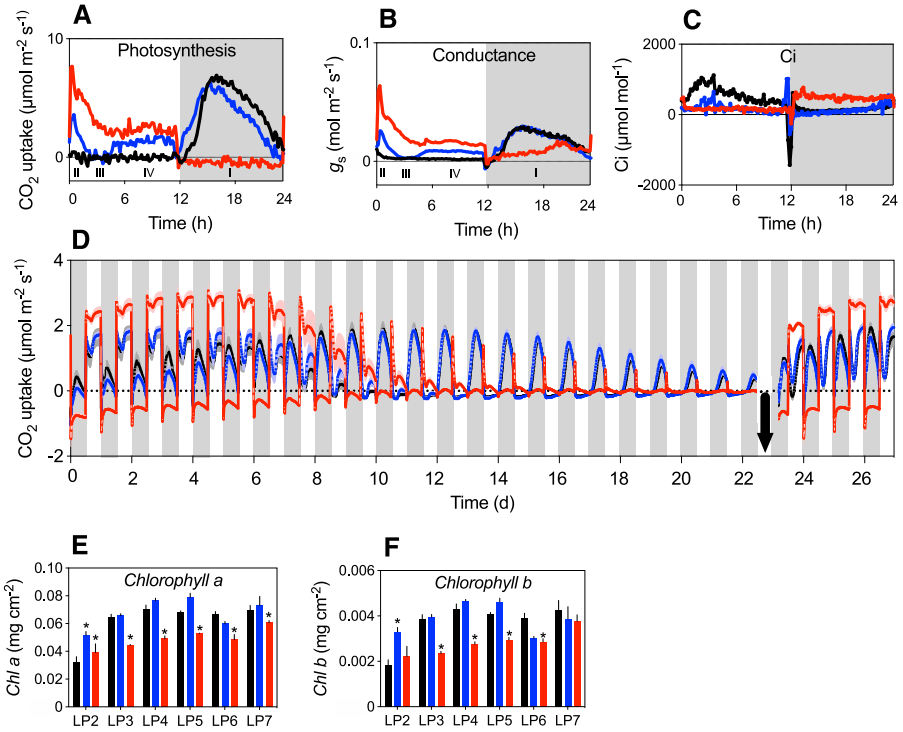

Figure 4. Impact of Silencing *PPC1* on 24-h Light/Dark Gas-Exchange Profiles under Well-Watered and Drought-Stressed Conditions and on Chlorophyll Content.

(A) to **(C)** CO_2 uptake profiles showing the four phases of CAM **(A)**, stomatal conductance (g_s) profile **(B)**, and the calculated internal partial pressure of CO_2 inside the leaf (C_i) profile **(C)** for CAM leaves (leaf pair 6 [LP6]) using plants pre-entrained for 7 d under 12-h-light/12-h-dark cycles.
(D) Impact of drought on *K. laxiflora* wild-type and transgenic lines with reduced *PPC1* expression. Gas-exchange profiles for shoots of whole young plants (nine-leaf-pair stage) measured throughout 27 d are shown. The plants were watered to full capacity on day 0 and allowed to progress into drought until day 23, when they were rewatered to full capacity (black arrow). The means for each of the four gas-exchange traces for each line are shown, with error bars showing the SE in the paler-colored extensions that extend above and below each of the data points.
(E) and **(F)** Impact of silencing *PPC1* on chlorophyll *a* **(E)** and chlorophyll *b* **(F)** contents in LP2 through LP7. The error bars represent the SE calculated for the three biological replicates, which were individual clones of each line. Asterisks indicate significant differences from the wild type based on Student's *t* test. For **(E)**, chlorophyll *a* in *rPPC1-A*, LP2, P = 0.000160; *rPPC1-B*, LP2, P = 0.043676; LP3, P = 0.000003; LP4, P = 0.000001; LP5, P = 0.000094; LP6, P = 0.000012; LP7, P = 0.010883. For **(F)**, chlorophyll *b* in *rPPC1-A*, LP2, P = 0.000304; *rPPC1-B*, LP3, P = 0.000019; LP4, P = 0.000016; LP5, P = 0.000653; LP6, P = 0.000951. All Student's *t* test parameters are presented in Supplemental Table 3. Black data are for the wild type, blue data for *rPPC1-A*, and red data for *rPPC1-B*.

The dark conductance of *rPPC1-B* corresponded with the release of respiratory CO_2 (Figure 4A). The calculated internal partial pressure of CO_2 inside the leaf was highest for the wild type in the light period, when stomata were closed, which is consistent with the expected high level of CO_2 inside the leaf during malate decarboxylation (Figure 4C). By contrast, in *rPPC1-B*, internal partial pressure of CO_2 inside the leaf peaked during the dark period, when stomata were slightly open, but the leaves failed to fix atmospheric CO_2 and respiratory CO_2 escaped (Figure 4C).

Impact of Drought on CO_2 Uptake in Plants Lacking *PPC1*

To test the importance of *PPC1* for carbon assimilation during drought, we measured CO_2 uptake continuously in whole, young plants (nine leaf pairs, 2 months old) over 22 d of drought, followed by rewatering (Figure 4D). The soil was watered to its holding capacity prior to placing the plants in the gas-exchange cuvettes at the start of the experiment, and then no further water was added until rewatering occurred on day 22. CAM develops with leaf age in *K. laxiflora*; the leaves gradually reduce light period CO_2 fixation and increase nocturnal CO_2 fixation as they mature (Supplemental Figure 4). A 2-month-old wild-type plant with nine leaf pairs thus includes young leaves fixing CO_2 mainly in the light via the C_3 pathway and older leaves fixing the majority of their atmospheric CO_2 in the dark via PPC and CAM.

When well-watered on day 1, the wild type, *rPPC1-A*, and *rPPC1-B* fixed, respectively, 7, 6, and −26% of their CO_2 during the dark period and 93, 94, and 126% during the light period (Table 1). This indicated that, in well-watered conditions, the young leaves of these young plants performed the majority of the 24-h CO_2 uptake (Table 1). On day 1, the wild type, *rPPC1-A*, and *rPPC1-B* fixed a total of 1093, 1008, and 1078 μmol atmospheric CO_2 m^{-2} over 24 h, respectively (Table 1). After 7 d without

watering, 24-h CO_2 fixation was 1345, 1367, and 1506 μmol m^{-2}, respectively. It should be noted that total leaf area was measured at the end of the experiment, so leaf growth and expansion during the experiment could not be accounted for.

After 7 d without water, there was a substantial increase in nocturnal CO_2 uptake in the wild type and *rPPC1-A* relative to day 1 (52 and 40% of CO_2 fixation occurred in the dark, respectively; Table 1). *rPPC1-B* respired less (−14%) after 7 d of drought relative to the −26% dark-respired CO_2 level on day 1 (Table 1). After 13 d of drought, the wild type, *rPPC1-A*, and *rPPC1-B* fixed, respectively, 795, 802, and 145 μmol CO_2 m^{-2} over the 24-h cycle (Table 1). Thus, plants performing CAM (the wild type and *rPPC1-A*) were able to fix over fivefold more CO_2 after 13 d of drought compared with *rPPC1-B*. Furthermore, after 22 d of drought, the wild type, *rPPC1-A*, and *rPPC1-B* fixed 76, 130, and −30 μmol m^{-2} during the 24-h light/dark cycle, respectively.

On day 22 without water, the drought-stressed plants were rewatered (see photographs in Supplemental Figure 3). After rewatering, CO_2 fixation increased rapidly for all plants (Figure 4D). In addition, the wild type and *rPPC1-A* displayed pronounced phase III of CAM after rewatering (Figure 4D). Following soil rehydration, the wild type fixed 931 μmol m^{-2} CO_2 in the dark compared with 768 μmol m^{-2} for *rPPC1-A*, whereas prior to drought, *rPPC1-A* fixed more atmospheric CO_2 (Table 1). *rPPC1-B* fixed CO_2 throughout the light period following rewatering, and it also resumed respiratory CO_2 loss throughout the dark period (Figure 4D).

As there was an increase in C_3 photosynthesis in *rPPC1-B*, we measured chlorophyll *a* and *b* levels in LP2 through LP7 (Figures 4E and 4F; Supplemental Table 3). Line *rPPC1-A* contained significantly more chlorophyll *a* and *b* than the wild type in LP2 (Figures 4E and 4F). *rPPC1-B* contained significantly more chlorophyll *a* than the wild type in LP2, significantly less chlorophyll *a* in LP3 through LP7, and significantly less chlorophyll *b* in LP3 to LP6 (Figures 4E and 4F). These decreased levels of chlorophyll *a* and *b* in LP3 to LP7 or LP6 in *rPPC1-B* were a surprising finding. In general, CAM species contain reduced levels of gene transcripts and encoded proteins associated with C_3 photosynthesis, such as Rubisco and light-harvesting complex components, when the level of CAM is induced by stress. Thus, reducing the level of CAM in LP3 through LP7 due to the silencing of *PPC1* was predicted to result in the induction of core C_3 photosynthesis genes and chlorophyll content in parallel with the measured increase in light period atmospheric CO_2 fixation via the C_3 pathway. Further elucidation of the reasons for this unexpected chlorophyll response may come from transcriptome-wide analysis of the differentially abundant transcripts in *rPPC1-B* compared with the wild type.

Characterization of CAM Gene Transcript Abundance in *rPPC1* Lines

Having established that *rPPC1-B* lacked nocturnal CO_2 fixation (Figure 4A), it was important to investigate the temporal regulation of other CAM-associated genes in the *rPPC1* RNAi lines. We investigated the transcript abundance of CAM genes in CAM leaves (LP6) using samples collected every 4 h over a 12-h-light/12-h-dark (LD) cycle (Figure 5). *PPDK* transcript levels were unchanged relative to the wild type in both *rPPC1* lines (Figure 5A), but its regulator gene *PPDK-RP* was upregulated in line *rPPC1-B* (Figure 5B), which is consistent with the continuous phosphorylation and inactivation of PPDK (Figures 2E and 2F). *β-NAD-ME* transcript levels appeared to be only slightly different from the wild

Table 1. Analysis of CO_2 Uptake in the Wild Type, *rPPC1-A*, and *rPPC1-B* during 22 d of Progressive Drought Stress and for 4 d following Rewatering

Line	Night 1	Day 1	Total Diel 1	Night 7	Day 7	Total Diel 7	Night 13	Day 13	Total Diel 13	Night 22	Day 22	Total Diel 22	Night 27	Day 27	Total Diel 27
Wild type (% of diel CO_2 uptake)	7	93	100	52	48	100	111	−11	100	133	−33	100	56	44	100
Wild type CO_2 uptake (μmol m^{-2})	78	1015	1093	698	647	1345	908	−113	795	152	−76	76	931	735	1666
rPPC1-A (% of diel CO_2 uptake)	6	94	100	40	60	100	112	−12	100	128	−28	100	46	54	100
rPPC1-A CO_2 uptake (μmol m^{-2})	73	1081	1008	553	814	1367	922	120	802	209	−81	130	768	889	1657
rPPC1-B (% of diel CO_2 uptake)	−26	126	100	−14	114	100	−6	106	100	−27	−73	100	−17	117	100
rPPC1-B CO_2 uptake (μmol m^{-2})	−575	1653	1078	−254	1759	1506	−17	161	145	−8	−22	−30	−385	1825	1440

Data are presented for selected days (1, 7, 13, 22, and 27) throughout the 27-d drought stress and rewatering experiment. Results expressed as percentages were calculated separately for the 12-h-light and 12-h-dark periods by determining the percentage of the total diel/24-h CO_2 uptake that occurred in that period. The actual CO_2 uptake over the 12-h-light and 12-h-dark period is also presented for each line.

type in the *rPPC1* lines but appeared to be lower in *rPPC1-B* at 22:00 h (Figure 5C).

In light of the marked reduction in starch to half the wild-type level in *rPPC1-B* (Figure 3B), we also measured transcripts associated with starch turnover. In *rPPC1-B*, dusk-phased starch breakdown-associated genes (*GWD*, *AMY3a* and *AMY3b*, and *PHS1*; Figures 5D to 5F and 5J) and sugar transporter genes (*MEX1* and *pGlcT*; Figures 5L and 5M) were upregulated, whereas dawn-phased starch breakdown genes (*BAM1*, *BAM3*, and *BAM9*; Figures 5G to 5I) and sugar transporter genes (*GPT2*; Figure 5K) were downregulated compared with the wild type.

Finally, a *CHLOROPHYLL A/B BINDING PROTEIN* (*CAB1*) gene was upregulated in *rPPC1-B* at dawn (Figure 5N), whereas a gene encoding a potential sucrose sensor connecting growth and

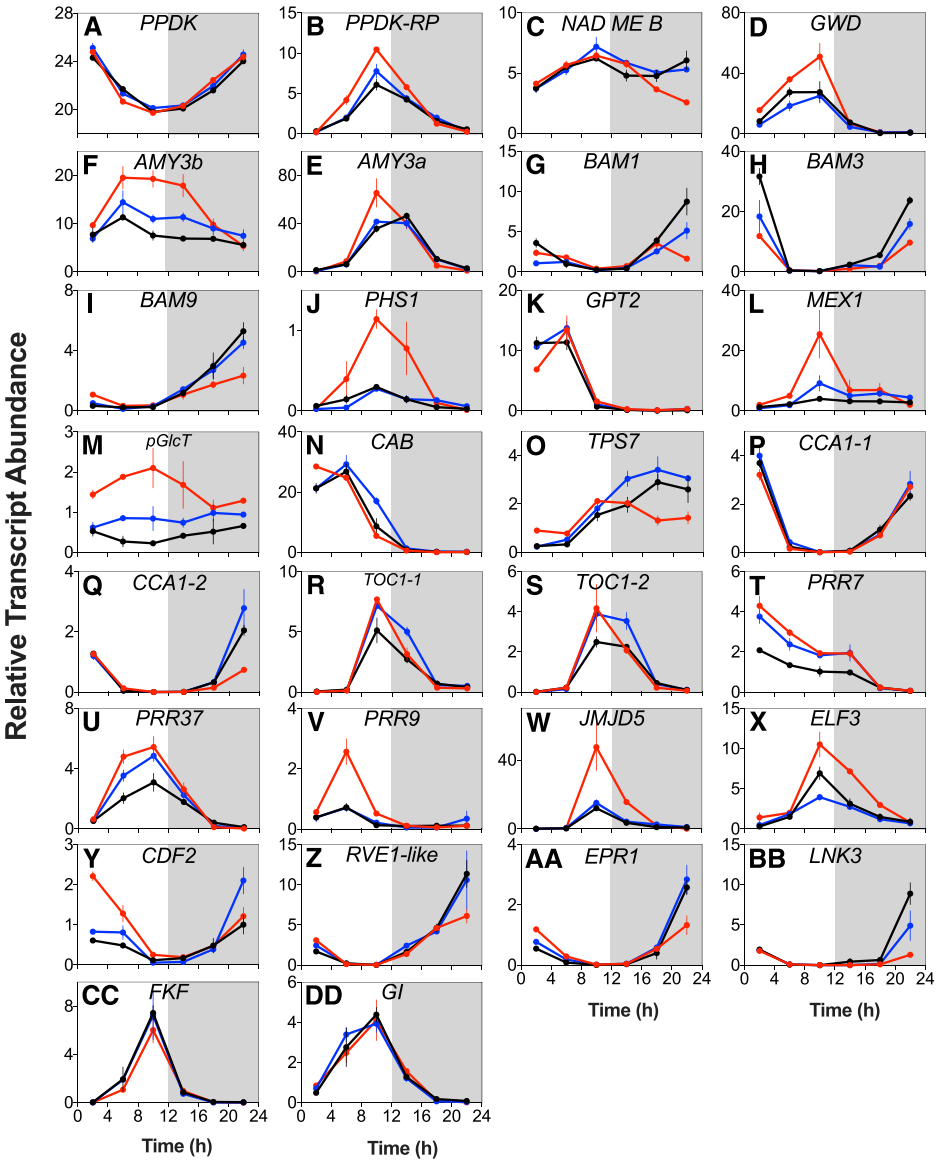

Figure 5. Impact of the Loss of *PPC1* Transcripts on the Light/Dark Regulation of the Transcript Abundance of CAM- and Central Circadian Clock-Associated Genes in RNAi Lines *rPPC1-A* and *rPPC1-B*.

Gene transcript abundance was measured using RT-qPCR for target genes *PPDK* **(A)**, *PPDK-RP* **(B)**, *β-NAD-ME* **(C)**, *GWD* **(D)**, *AMY3a* **(E)**, *AMY3b* **(F)**, *BAM1* **(G)**, *BAM3* **(H)**, *BAM9* **(I)**, *PHS1* **(J)**, *GPT2* **(K)**, *MEX1* **(L)**, *pGlcT* **(M)**, *CAB* **(N)**, *TPS7* **(O)**, *CCA1-1* **(P)**, *CCA1-2* **(Q)**, *TOC1-1* **(R)**, *TOC1-2* **(S)**, *PRR7* **(T)**, *PRR3/7* **(U)**, *PRR9* **(V)**, *JMJ30/JMJD5* **(W)**, *ELF3* **(X)**, *CDF2* **(Y)**, *RVE1-like* **(Z)**, *EPR1* **(AA)**, *LNK3* **(BB)**, *FKF1* **(CC)**, and *GI* **(DD)**. Mature leaves (LP6) were sampled every 4 h across the 12-h-light/12-h-dark cycle. A thioesterase/thiol ester dehydrase-isomerase superfamily gene (*TEDI*) was amplified from the same cDNAs as a reference gene. Gene transcript abundance data represent means of three technical replicates for biological triplicates and were normalized to the loading control gene (*TEDI*); error bars represent the SE. In all cases, plants were entrained under 12-h-light/12-h-dark cycles for 7 d prior to sampling. Black data are for the wild type, blue data for *rPPC1-A*, and red data for *rPPC1-B*.

development to metabolic status, *TREHALOSE 6-PHOSPHATE SYNTHASE7* (*TPS7*; Schluepmann et al., 2003), was downregulated relative to the wild type at 6 and 10 h into the 12-h-dark period (Figure 5O).

Characterization of Diel Regulation of Circadian Clock Genes in *rPPC1* Lines

Recent studies using *PPCK1* RNAi lines in *Kalanchoë* reported that a reduced temporal peak of sucrose content phased to 2 h after dawn correlated with perturbation of the central circadian clock (Boxall et al., 2017). Of the two *CIRCADIAN CLOCK ASSOCIATED1* (*CCA1*) genes in *K. laxiflora*, each of which is represented by two homeologous copies in the tetraploid genome, only the two homeologs of *CCA1-2* were downregulated in *rPPC1-B* (Figures 5P and 5Q), whereas both homeologs of both *TIMING OF CHLOROPHYLL A/B BINDING PROTEIN1* (*TOC1*) genes were upregulated in both *rPPC1-A* and *rPPC1-B* (Figures 5R and 5S). Two other pseudoresponse regulators (*PRRs*) related to *TOC1*, namely *PRR7* and *PRR3/7*, were upregulated in both *rPPC1-A* and *rPPC1-B* (Figures 5T and 5U), and *PRR9* was induced almost fivefold in the middle of the light period, specifically in line *rPPC1-B* (Figure 5V).

Other-clock associated genes, including *JUMONJI DOMAIN CONTAINING30/5* (*JMJ30/JMJD5*), *EARLY FLOWERING3* (*ELF3*), and *CYCLING DOF-FACTOR2* (*CDF2*), were also upregulated in line *rPPC1-B* (Figures 5W to 5Y) versus the wild type, whereas the single MYB-repeat transcription factor genes *REVEILLE1-like* (*RVE1-like*) and *EARLY-PHYTOCHROME-RESPONSIVE1* (*EPR1*) as well as *LIGHT NIGHT-INDUCIBLE AND CLOCK-REGULATED3-like* (*LNK3-like*) were downregulated (Figure 5Z to 5BB). Finally, *CCA1-1*, *FLAVIN BINDING KELCH-REPEAT F-BOX PROTEIN1* (*FKF1*), and *GIGANTEA* (*GI*) transcript levels were consistent among all three lines (Figures 5P, 5CC, and 5DD).

Gas-Exchange Characteristics of *rPPC1* Lines under Circadian Free-Running Conditions

Under LL free-running conditions, detached *K. laxiflora* wild-type CAM leaves (LP6) with their petioles in water displayed a robust circadian rhythm of CO_2 uptake with a period of ~20 h (Figure 6A). This rhythm was entirely consistent with CAM rhythms reported previously for detached LP6 of closely related *Kalanchoë* species with obligate CAM (Lüttge and Ball, 1978; Anderson and Wilkins, 1989). The rhythm dampened rapidly in line *rPPC1-B*, whereas *rPPC1-A* maintained a rhythm that was very similar to that of the wild type (Figure 6A).

When LL CO_2 uptake was measured for well-watered whole plants (2 months old, nine leaf pairs), *rPPC1-B* fixed more CO_2 than the wild type and line *rPPC1-A*, with levels of 11,269, 7414, and 8383 μmol CO_2 m^{-2}, respectively (Figure 6B). The wild type maintained robust oscillations of CO_2 exchange under LL conditions, whereas *rPPC1-A* dampened to arrhythmia after 3 d and *rPPC1-B* was arrhythmic (Figure 6B). It should be noted that the LL CO_2-exchange data for intact young plants with their roots in soil (Figure 6B) differ from the data for detached LP6 (Figure 6A) because the whole plants measured in Figure 6B included leaf pairs from very young LP1, which perform C_3, through to LP6 to LP9, which perform full CAM (phase I in the dark and phase III in the light). The detached LP6 measured in Figure 6A were full CAM leaves only, at least for the wild type (Supplemental Figure 4). Thus, the more rapid and substantial dampening of the free-running CO_2 fixation rhythm toward arrhythmia in lines *rPPC1-A* and *rPPC-1B* relative to the wild type (Figure 6B) suggests that the younger leaves (LP1 to LP5) made a dominant contribution to the robust circadian rhythm in wild-type whole plants.

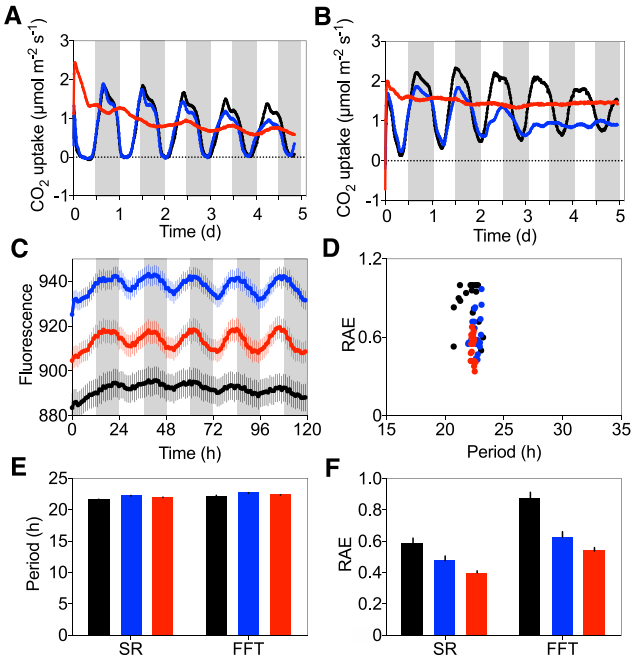

Figure 6. Effects of Silencing *PPC1* on CAM CO_2-Exchange Rhythms Measured under LL Conditions.

(A) Gas-exchange profile for detached CAM leaves (LP6) was measured using leaves entrained under a 12-h-light/12-h-dark cycle followed by release into constant LL conditions (100 μmol m^{-2} s^{-1} at 15°C).

(B) Gas-exchange profile for well-watered whole young plants (nine-leaf-pair stage) using plants entrained under 12-h-light/12-h-dark cycles followed by release into constant LL conditions (100 μmol m^{-2} s^{-1} at 15°C). The data in **(A)** and **(B)** represent mean CO_2 uptake of three individual plants.

(C) DF circadian rhythms became more robust in lines *rPPC1-A* and *rPPC1-B*. Plants were entrained under 12-h-light/12-h-dark cycles before being transferred to constant red-blue light (35 μmol m^{-2} s^{-1}) under the CCD imaging camera system. DF was assayed with a 1-h time resolution for 120 h. The plots represent normalized averages for DF measured for 21 leaf discs sampled from three biological replicates of LP6 from each line. Error bars indicate SE calculated from three biological replicates.

(D) RAE plot for the DF rhythms.

(E) and **(F)** Mean period length plot **(E)** and mean RAE plot **(F)**. The plotted values were calculated using the BioDare package for circadian rhythm analysis. FFT, fast Fourier transform-nonlinear least squares analysis; SR, spectral resampling analysis.

For all panels, black data are for the wild type, blue data for *rPPC1-A*, and red data for *rPPC1-B*. LL begins at 0 h in **(A)** to **(C)**.

DF Rhythms Are Enhanced in *rPPC1-B* Despite the Loss of CAM-Associated CO_2 Uptake Rhythms

DF displays a robust circadian rhythm in *Kalanchoë* and provides a measure of a chloroplast-derived clock output that can be used for statistical analysis of circadian period, robustness, and accuracy (Gould et al., 2009; Boxall et al., 2017). We therefore measured and analyzed DF under LL (Figure 6C) to calculate rhythm statistics using BioDare (Moore et al., 2014; Zielinski et al., 2014).

Wild-type DF oscillations were very similar to those reported previously for *K. fedtschenkoi* (Figure 6C; Gould et al., 2009; Boxall et al., 2017). *rPPC1-A* and *rPPC1-B* had more robust oscillations than the wild type (Figure 6C). The rhythm amplitude increased slightly with time in *rPPC1-A* and *rPPC1-B* but remained relatively constant in the wild type. The relative amplitude error (RAE) plot showed a wider spread of period for the wild type than for the *rPPC1* lines (Figure 6D). Mean periods were between 21.5 and 22.1 h when calculated using spectral resampling or fast Fourier transform (nonlinear least squares) methods, respectively (Figure 6E). Average periods were similar between the wild type and the *rPPC1* lines. A lower mean RAE was calculated for *rPPC1-A* and *rPPC1-B* compared with the wild type (Figure 6F), supporting statistically the visibly robust and high-amplitude DF rhythm in the *rPPC1* lines (Figure 6C).

Rhythm Characteristics of Core Circadian Clock and Clock-Controlled Genes

Having established that circadian control of CO_2 fixation was dampened under LL in plants lacking *PPC1*, whereas the circadian control of DF was enhanced under LL (Figures 6A to 6F), it was important to investigate the regulation of both core clock genes and circadian clock-controlled genes in the *rPPC1* lines under LL (Figure 7).

The wild type displayed a rhythm in the transcript abundance of *PPC1* that was absent in *rPPC1-B* (Figure 7A). *PPC2* was rhythmic in the wild type and *rPPC1-B*, but its abundance was lower in *rPPC1-B* (Figure 7B). The *PPCK1* rhythm was of greater amplitude in *rPPC1-B*, and the daily transcript peaks occurred 4 to 8 h later than in the wild type after the first 24 h of LL (Figure 7C). *PPCK2* and *PPCK3* were induced in line *rPPC1-B* and oscillated with higher amplitude (Figures 7D and 7E). *PPCK2* peaked after the wild type on the second and third 24-h cycles under LL (Figures 7D and 7E), which is consistent with the induction detected under light/dark cycles (Figures 1F and 1G). *GPT2*, which is involved in the transport of G6P across the chloroplast membrane, was downregulated and had lower amplitude in *rPPC1-B* than the wild type (Figure 7F), whereas *CAB1* was induced and oscillated robustly (Figure 7G).

In *rPPC1-B*, the core clock gene *CCA1-1* was downregulated, phase delayed, and had lower amplitude than the wild type (Figure 7H), whereas *CCA1-2*, *TOC1-1*, and *TOC1-2* were all upregulated and phase delayed relative to the wild type for the latter two peaks of LL (Figures 7I to 7K). *PRR7* was upregulated and more robustly rhythmic in *rPPC1-B* (Figure 7L), whereas the rhythms of *PRR3/7* and *PRR9* dampened in *rPPC1-B* (Figures 7M and 7N). Finally, *JMJ30/JMJD5*, *ELF3*, *CDF2*, *RVE1-like*, *EPR1*, *FKF1*, and *GI* were upregulated in *rPPC1-B*, displaying higher amplitude, phase delays, and/or period lengthening during the LL time course (Figures 7P to 7V), whereas *LNK3-like* was downregulated but remained rhythmic, with a lengthening period compared with the wild type (Figure 7O).

Diel Regulation of GC Signaling and Ion Channel Genes in GC-Enriched Epidermal Peels of *rPPC1-B*

As CO_2 fixation and associated stomatal opening were shifted to the light period in *rPPC1-B*, it was important to investigate the temporal regulation of known GC signaling genes in the wild type and the *rPPC1-B* line (Figure 8). Since epidermal peels of *Kalanchoë* leaves are enriched for intact GCs, we isolated RNA from epidermal peels from the upper and lower leaf surfaces of LP6 every 4 h over the LD cycle and used them for RT-qPCR.

PHOTOTROPIN1 (*PHOT1*) encodes a protein kinase that acts as a blue light (BL) photoreceptor in the signal transduction pathway leading to BL-induced stomatal movements (Kinoshita et al., 2001). In *rPPC1-B*, *PHOT1* transcripts were upregulated relative to the wild type and peaked 8 h into the 12-h-light period (Figure 8A). *CRYPTOCHROME2* (*CRY2*) encodes a photoreceptor that regulates BL responses, including the entrainment of endogenous circadian rhythms (Somers et al., 1998), and stomatal conductance via an indirect effect on ABA levels (Boccalandro et al., 2012). In *rPPC1-B* epidermal peels, *CRY2* transcript levels were upregulated and peaked at dusk, whereas *CRY2* peaked 8 h into the dark in the wild type (Figure 8B).

In Arabidopsis, GC-localized β-CARBONIC ANHYDRASE1 (CA1) and CA4 are involved in CO_2 sensing in GCs, with the *ca1 ca4* mutant displaying impaired stomatal control in response to CO_2 (Hu et al., 2010). In *rPPC1-B*, a β-carbonic anhydrase gene was much more strongly induced at dawn relative to the wild type (Figure 8C). PATROL1 controls the tethering of the proton ATPase AHA1 to the plasma membrane and is essential for stomatal opening in response to low CO_2 and light levels (Hashimoto-Sugimoto et al., 2013). The cycle of *PATROL1* in epidermal peels was slightly different between *rPPC1-B* and the wild type, with *rPPC1-B* peaking 4 h into the dark but the wild type peaking at 4 h into the light period (Figure 8D).

CONVERGENCE OF BLUE LIGHT AND CO_2 1/2 (CBC1/2) stimulate stomatal opening by inhibiting S-type anion channels in response to both BL and low CO_2 and connect BL signals perceived by PHOT1 with the protein kinase HIGH LEAF TEMPERATURE1 (HT1; Hiyama et al., 2017). Both proteins interact with and are phosphorylated by HT1. In *rPPC1-B*, *CBC1/2* was upregulated compared with the wild type both in the second half of the dark period and at dawn (Figure 8E). HT1 acts as a negative regulator of high-CO_2-induced stomatal closure (Hashimoto et al., 2006). *HT1* transcript levels were reduced throughout the light/dark cycle relative to the wild type in *rPPC1-B* (Figure 8F). *OPEN STOMATA1* (*OST1*), encoding a protein kinase that acts downstream of HT1 (Imes et al., 2013), was upregulated in *rPPC1-B* both at 8 h into the dark period and at dawn, the time of the daily trough in the wild type (Figure 8G).

Genes involved in ion transport across the plasma membrane and tonoplast play a crucial role in the changes in cell turgor pressure that drive stomatal movements (Jezek and Blatt, 2017). SLOW

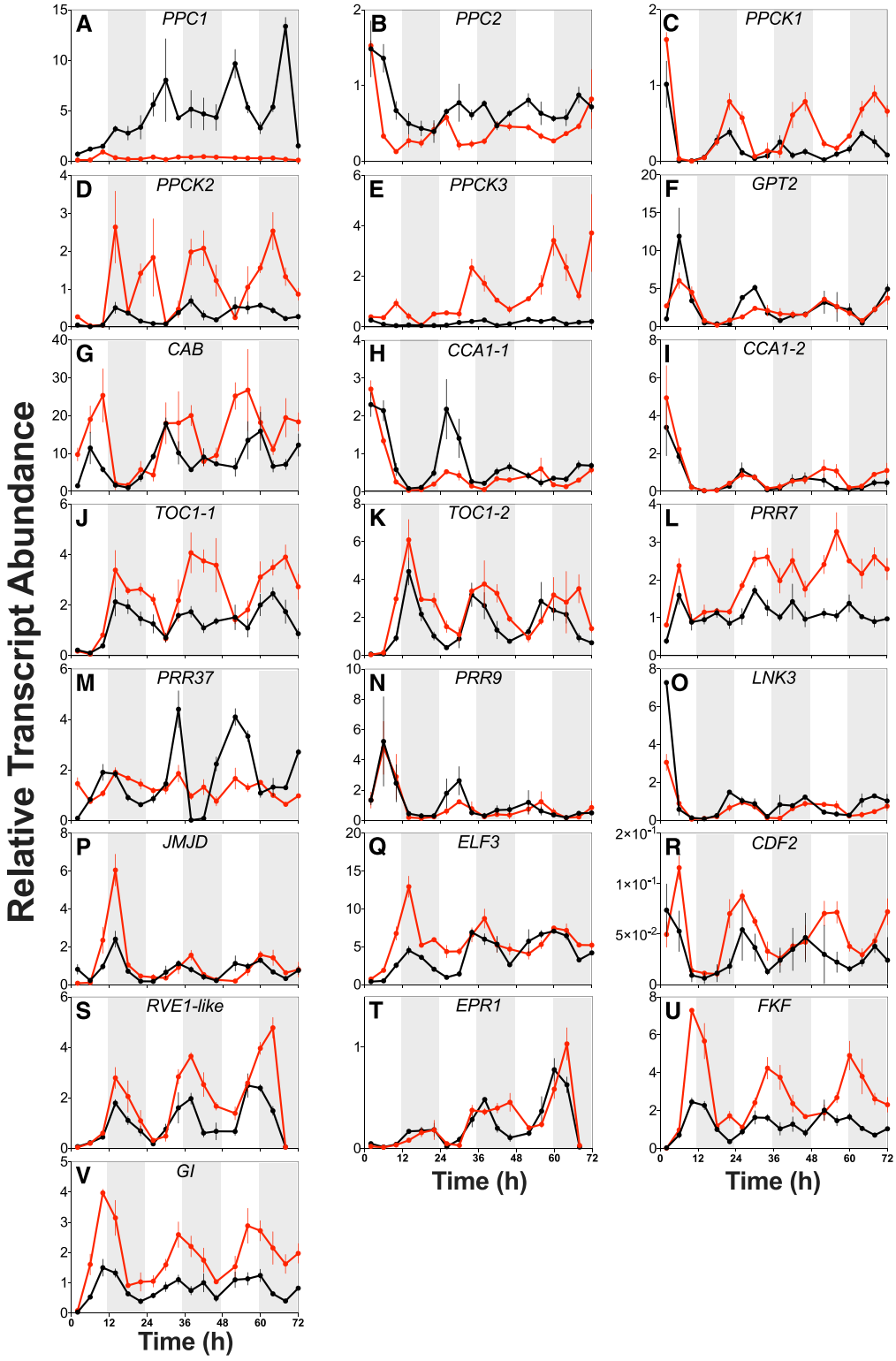

Figure 7. Impact of the Loss of *PPC1* Transcripts on Circadian Clock-Controlled Gene Transcript Abundance during LL Free-Running Conditions.

Mature leaves (LP6), which performed CAM in the wild type, were sampled every 4 h under constant LL conditions (100 μmol m^{-2} s^{-1} at 15°C) for the wild type and *rPPC1-B*. RNA was isolated and used for RT-qPCR. A thioesterase/thiol ester dehydrase-isomerase superfamily gene (*TEDI*) was amplified as a reference gene from the same cDNAs. Gene transcript abundance data represent means of three technical replicates for biological triplicates and were

ACTIVATED ANION CHANNEL1 (SLAC1) is a key player in the closure of stomata in response to high CO_2 concentrations (Hedrich and Geiger, 2017). SLAC1 is regulated by ABA signaling, which requires dephosphorylation steps catalyzed by PP2C. In *rPPC1-B*, *SLAC1* was upregulated and peaked during the light (Figure 8H) and *PP2C* was upregulated relative to the wild type during the dark period (Figure 8I). ABA is recognized and bound by the REGULATORY COMPONENT OF ABA RECEPTORS (RCARs)/PYRABACTIN RESISTANCE1, which interact with PP2C to stimulate ABA signaling (Ma et al., 2009; Park et al., 2009; Santiago et al., 2009). In *rPPC1-B* epidermal peels, *RCAR3* transcripts were induced spanning dusk and the first half of the dark period and peaked at least 4 h earlier than in the wild type (Figure 8J).

In *rPPC1-B*, the transcript level of *GUARD CELL OUTWARD RECTIFYING K^+ CHANNEL* (*GORK*), which is involved in regulating stomatal movement according to water status (Ache et al., 2000), peaked 4 h earlier than in the wild type (Figure 8K). *STELAR K^+ OUTSIDE RECTIFIER* (*SKOR*) encodes a selective outward-rectifying potassium channel (Gaymard et al., 1998). *SKOR* transcript levels peaked at dawn in the wild type, whereas in *rPPC1-B*, *SKOR* transcript levels reached their daily minimum at dawn (Figure 8L). The transcript level of plasma membrane-localized *ALUMINUM ACTIVATED MALATE TRANSPORTER12* (*ALMT12*), which is involved in dark-, CO_2-, ABA-, and water deficit-induced stomatal closure, was elevated relative to the wild type at dawn in *rPPC1-B* (Figure 8M). The E3 UBIQUITIN-PROTEIN LIGASE RMA1 promotes the ubiquitination and proteasomal degradation of the aquaporin PIP2:1, which plays a role in GC regulation (Grondin et al., 2015). *RMA1* was induced threefold at dawn in *rPPC1-B* compared with the wild type (Figure 8N). EMBRYO SAC DEVELOPMENT ARREST39 (EDA39) is a calmodulin binding protein that promotes stomatal opening (Zhou et al., 2012). In *rPPC1-B*, *EDA39* was upregulated relative to the wild type and peaked at dusk (Figure 8O).

SALT OVERLY SENSITIVE2 (SOS2) is a Calcineurin B-Like-interacting protein kinase involved in the regulatory pathway for intracellular Na^+ and K^+ homeostasis and salt tolerance (Liu et al., 2000). SOS2 interacts with and activates the vacuolar H^+/Ca^{2+} antiporter CAX1, thereby functioning in cellular Ca^{2+} homeostasis, an important function during stomatal opening and closing (Cheng et al., 2004). *SOS2* transcript levels were elevated relative to the wild type at all time points; in particular, it was induced approximately fivefold at its peak 4 h into the dark period in epidermal peels of *rPPC1-B* relative to the wild type (Figure 8P). Ca^{2+}-ATPase2 (ACA2) and ENDOMEMBRANE-TYPE Ca^{2+}-ATPASE4 (ECA4) catalyze the hydrolysis of ATP coupled with the translocation of calcium from the cytosol into the endoplasmic reticulum and/or an endomembrane compartment (Jezek and Blatt, 2017). *ACA2* and *ECA4* were induced by approximately fourfold to approximately eightfold in *rPPC1-B* epidermal peels relative to the wild type, particularly when they reached peak levels at 4 h into the 12-h-dark period (Figures 8Q and 8R).

Finally, the transcription factor MYB60 is involved in stomatal opening in response to light and promotes GC deflation in response to water deficit (Cominelli et al., 2005). In *rPPC1-B*, *MYB60* was induced approximately fivefold relative to the wild type at dawn, although it also maintained a dusk-phased peak of transcript abundance like the wild type (Figure 8S). MYB61 functions as a transcriptional regulator of stomatal closure (Liang et al., 2005). *MYB61* was downregulated in *rPPC1-B* relative to the wild type and peaked 8 h later in *rPPC1-B*, 4 h into the dark period, whereas in the wild type, *MYB61* peaked in the light 4 h before dusk (Figure 8T).

Diel Regulation of GC Metabolism Genes in GC-Enriched Epidermal Peels of *rPPC1-B*

PPC1 and *PPC2* transcript levels were low in epidermal peels (Supplemental Figures 5A and 5B) compared with whole leaves (Figure 1A). *PPC3* and *PPC4* transcripts were more abundant in wild-type epidermal peels (Supplemental Figures 5C and 5D) relative to whole leaves (Figures 1C and 1D). Furthermore, *PPC3* and *PPC4* were upregulated in epidermal peels of *rPPC1-B* compared with the wild type, and their transcript abundance peaked 4 h into the dark period, whereas in the wild type, the abundance of both transcripts peaked at the end of the dark period or dawn (Supplemental Figures 5A to 5D).

CAM-specific *PPCK1* was upregulated in *rPPC1-B* epidermal peels compared with the wild type, whereas the expression of *PPCK2*, which does not currently have a proposed role in the regulation of CAM-specific *PPC1* in the mesophyll, was unchanged (Supplemental Figures 5E and 5F). Both *PPCK2* and *PPCK3* transcripts were more abundant than *PPCK1* in epidermal peels, suggesting that their encoded proteins might regulate the activity of the GC PPCs (Supplemental Figures 5F and 5G). Most strikingly, *PPCK3* was upregulated approximately fivefold at 4 h after lights-on in *rPPC1-B* epidermal peels relative to the wild type (Supplemental Figure 5G).

In C_3 plants, starch is degraded before dawn to fuel stomatal opening (Blatt, 2016). In Arabidopsis GCs, *BAM1* encodes the major starch-degrading enzyme (Valerio et al., 2011; Prasch et al., 2015; Horrer et al., 2016; Santelia and Lunn, 2017) that functions with AMY3 to mobilize starch at dawn, releasing maltose in the chloroplasts (Horrer et al., 2016). In *rPPC1-B* epidermal peels, *GWD* transcript levels were halved relative to the wild type at its peak (i.e., 8 h into the 12-h light period; Supplemental Figure 5H). *AMY3a* and *AMY3b* were upregulated at dusk and in the second half of the light period, respectively (Supplemental Figures 5I and

Figure 7. (continued).

normalized to the loading control gene (*TEDI*); error bars represent the SE. In all cases, plants were entrained under 12-h-light/12-h-dark cycles prior to release into LL free-running conditions at 0 h. Black data are for the wild type and red data for *rPPC1-B*. The gray bars behind the data represent the subjective dark period, the time when it would have been dark under the previous entrainment conditions. Likewise, the white regions represent the subjective light period. Panels show the circadian rhythm of transcript abundance under constant LL conditions (100 μmol m^{-2} s^{-1} at 15°C) for the wild type and *rPPC1-B* for *PPC1* **(A)**, *PPC2* **(B)**, *PPCK1* **(C)**, *PPCK2* **(D)**, *PPCK3* **(E)**, *GPT2* **(F)**, *CAB* **(G)**, *CCA1-1* **(H)**, *CCA1-2* **(I)**, *TOC1-1* **(J)**, *TOC1-2* **(K)**, *PRR7* **(L)**, *PRR37* **(M)**, *PRR9* **(N)**, *LNK3-like* **(O)**, *JMJ30/JMJD5* **(P)**, *ELF3* **(Q)**, *CDF2* **(R)**, *RVE1-like* **(S)**, *EPR1* **(T)**, *FKF1* **(U)**, and *GI* **(V)**.

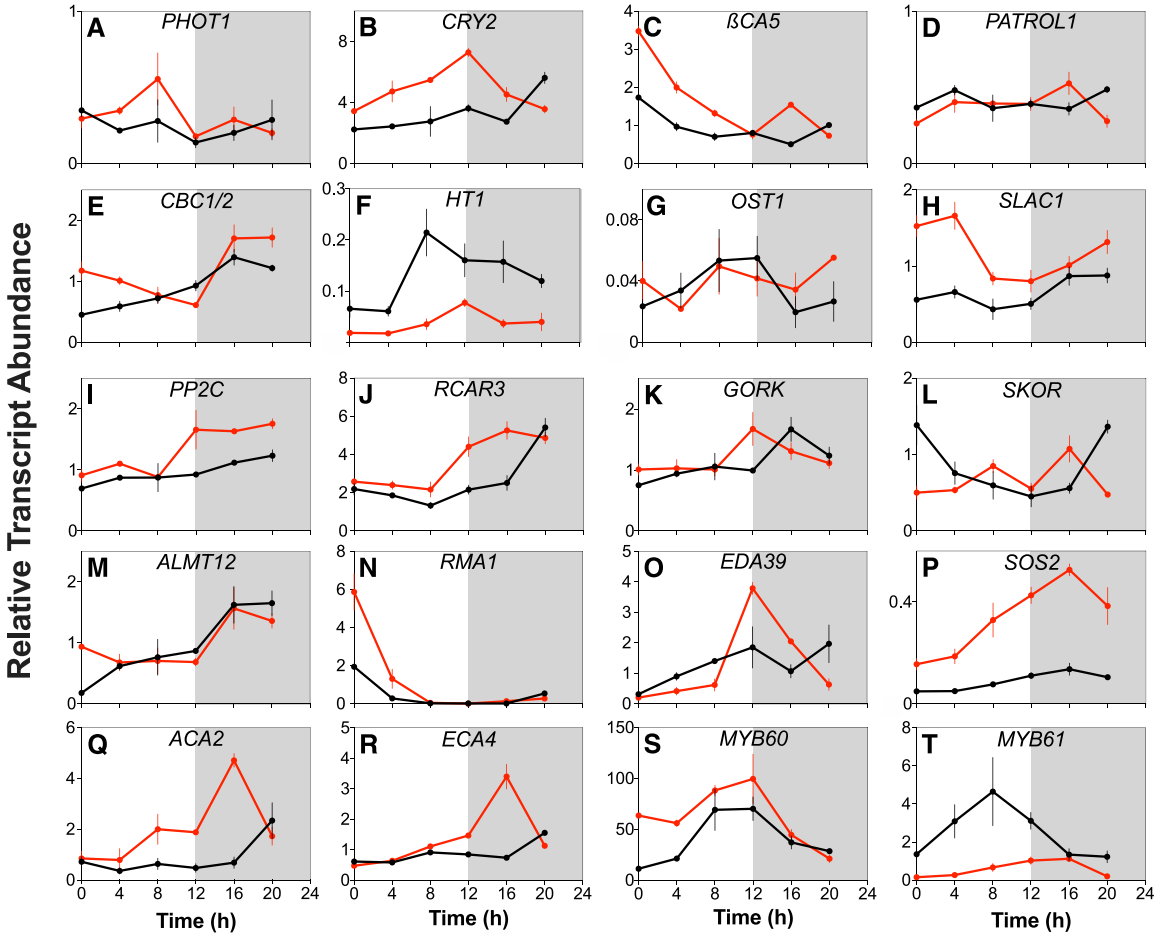

Figure 8. Impact of the Loss of PPC Activity on the Light/Dark Regulation of the Transcript Abundance of Stomatal Genes in the Epidermis.

Plants were entrained under 12-h-light/12-h-dark conditions for 7 d prior to sampling. Epidermal peel samples were separated from LP6, LP7, and LP8, with samples collected every 4 h starting at 02:00 h, 2 h into the 12-h-light period. Each biological sample represents a pool of epidermal peels taken from six LP6 leaves from three clonal stems of each line. Each peel was frozen in liquid nitrogen immediately after it was taken and pooled later. RNA was isolated and used in RT-qPCR. A thioesterase/thiol ester dehydrase-isomerase superfamily gene (*TEDI*) was amplified as a reference gene from the same cDNAs. Gene transcript abundance data represent means of three technical replicates for biological triplicates and were normalized to the reference gene (*TEDI*); error bars represent the SE. In all cases, plants were entrained under 12-h-light/12-h-dark cycles for 7 d prior to sampling. Black data are for the wild type and red data for *rPPC1-B*. Panels show the light/dark regulation of transcript abundance under constant LL conditions (100 μmol m^{-2} s^{-1} at 15°C) for the wild type and *rPPC1-B* for *PHOT1* **(A)**, *CRY2* **(B)**, *βCA5* **(C)**, *PATROL1* **(D)**, *CBC1/2* **(E)**, *HT1* **(F)**, *OST1* **(G)**, *SLAC1* **(H)**, *PP2C* **(I)**, *RCAR3* **(J)**, *GORK* **(K)**, *SKOR* **(L)**, *ALMT12* **(M)**, *RMA1* **(N)**, *EDA39* **(O)**, *SOS2* **(P)**, *ACA2* **(Q)**, *ECA4* **(R)**, *MYB60* **(S)**, and *MYB61* **(T)**.

5J). *BAM1* was upregulated at dawn compared with the wild type and peaked with a very similar transcript abundance to the wild type at 20:00 h, 8 h into the dark period (Supplemental Figure 5K), whereas *BAM3* transcript levels were approximately threefold lower in *rPPC1-B* relative to the wild type at the time of its nocturnal peak, which also occurred 8 h into the dark (Supplemental Figure 5L). *BAM9* expression in *rPPC1-B* rose later than in the wild type, lagging behind the wild type at dusk and 4 h into the dark, and it stayed approximately fivefold higher at dawn and 4 h into the light period, when the wild type reached its daily trough (Supplemental Figure 5M). BAM9 in Arabidopsis is predicted to be catalytically inactive and has no known function to date (Monroe and Storm, 2018). The peak of *PHS1* was delayed by 4 h, peaking at the light/dark transition (Supplemental Figure 5N), and *MEX1* was downregulated in epidermal peels of *rPPC1-B*, peaking at 08:00 h in the light, 4 h after the wild-type peak (Supplemental Figure 5O).

Diel Regulation of Core Circadian Clock Genes in Epidermal Peels of *rPPC1-B*

The circadian clock genes *PRR3/7* and *PRR7* were upregulated in epidermal peels of *rPPC1-B* relative to the wild type (Supplemental Figures 5P and 5Q), with a similar diel pattern to that measured in whole CAM leaves (Figures 5S and 5T). *PRR3/7* peaked 4 h earlier in *rPPC1-B*, whereas *PRR7* transcript levels were greater throughout the light period in *rPPC1-B* (Supplemental Figures 5P and 5Q). *LUX* is a component of the morning transcriptional feedback circuit within the clock, encoding a transcription factor

that directly regulates the expression of *PRR9* by binding to specific sites in its promoter (Helfer et al., 2011). In epidermal peels, *LUX* was downregulated greater than sevenfold in *rPPC1-B* compared with the wild type at its peak, 4 h into the light period, and also peaked 4 h later than the wild type (Supplemental Figure 5R).

Diel Regulation of Additional GC Signaling Genes in GC-Enriched Epidermal Peels of *rPPC1-B*

GCs perceive CO_2 and regulate stomatal aperture via ABA and reactive oxygen species signaling, with low CO_2 levels mediating stomatal opening and high CO_2 levels causing closure (Chater et al., 2015). *NADP OXIDOREDUCTASE* encodes an NADP binding Rossman-fold superfamily protein that we only detected in epidermal peels in *Kalanchoë*. The enzyme encoded by this gene might generate the H_2O_2 burst induced by ABA as part of the stomatal closure signaling pathway (Daszkowska-Golec and Szarejko, 2013). This transcript was upregulated approximately threefold in *rPPC1-B* at dawn (Supplemental Figure 5S).

In Arabidopsis, the transcription factors MYB94 and MYB96 function together in the activation of cuticular wax biosynthesis under drought stress (Lee et al., 2016). MYB96 may also be involved in the response to drought stress in Arabidopsis through ABA signaling that mediates stomatal closure via the *RD22* pathway (Seo et al., 2011). Both *MYB94* and *MYB96* were induced by as much as threefold in *rPPC1-B* compared with the wild type (Supplemental Figures 5T and 5U). Specifically, *MYB94* transcript levels rose 8 h earlier than they did in the wild type and were already close to peak levels by the light-to-dark transition, whereas in the wild type, *MYB94* levels peaked sharply 8 h into the dark period (Supplemental Figure 5T). *MYB96* transcription was induced relative to the wild type at both dawn and dusk, but the peak of *MYB96* transcription at dawn represented the largest fold change relative to the wild type (Supplemental Figure 5U).

DISCUSSION

CAM Provides a Selective Advantage in the Face of Drought

The data presented here for CO_2 fixation during progressive drought demonstrate very clearly the importance of a fully functional CAM system for continued atmospheric CO_2 fixation throughout a period of drought lasting just over 3 weeks (Figure 4D). Although the intermediate line *rPPC1-A* continued to perform atmospheric CO_2 fixation and malate accumulation in the dark and stomatal closure in the light period, it was less able to adapt to drought by inducing CAM compared with the wild type. Thus, by comparing the impacts of the different levels of *PPC1* silencing in these transgenic lines of *Kalanchoë*, it is possible to conclude that the wild-type level of *PPC1* transcript enables the plant to adapt to drought more rapidly by increasing nocturnal CO_2 fixation and malate accumulation and by decreasing the magnitude and duration of phases II and IV of CAM in the light. These swift adaptations allow the wild type to curtail excessive water loss more rapidly than either of the transgenic lines with reduced *PPC1* transcript levels, suggesting that the high level of *PPC1* transcript in the wild type provides a genuine adaptive advantage in terms of allowing the plant to prevent excessive water loss during gradual soil drying.

Upon rewatering on day 23, both wild-type and *rPPC1-A* plants returned to performing strong, four-phase CAM, including pronounced phase II and IV at the start and end of the light period, respectively (Figure 4D). Line *rPPC1-B* also bounced back to its normal, predrought physiology after rewatering, which is consistent with the rewatering response reported previously for a range of facultative, weak-CAM species, including *M. crystallinum*, purslane (*Portulaca oleracea*), *Portulaca umbraticola*, *T. triangulare*, and various *Calandrinia* species (Winter and Holtum, 2014; Holtum et al., 2017; Winter, 2019). Overall, the response of *rPPC1-B* to progressive drought stress and subsequent rewatering is reminiscent of the physiological response of facultative CAM species such as *T. triangulare* and *M. crystallinum*, although both of these true facultative CAM species did achieve net atmospheric CO_2 fixation in the dark period following ~12 to 13 d of drought (Winter and Holtum, 2014).

Although the *rPPC1-B* plants fixed all of their CO_2 in the light, especially during a pronounced and extended phase II in the hours after dawn, the CO_2-uptake pattern was not constant over the light period (Figure 4A). For example, in LP6 of a well-watered plant, CO_2 fixation dropped from ~8 μmol m^{-2} s^{-1} during phase II after dawn to ~2 to 3 μmol m^{-2} s^{-1} around 4 h after lights-on (Figure 4A), and stomatal conductance decreased to a similar extent (Figure 4B). The observed stomatal closure could not have been due to a high malate concentration and associated internal release of CO_2 in the mesophyll (Figure 3A). These data are consistent with the current hypothesis that a signal from the core circadian clock drives the closure of CAM stomata in the light and the associated decline in atmospheric CO_2 fixation, even when a CAM leaf has not produced malate during the preceding dark period (von Caemmerer and Griffiths, 2009).

Overall, with respect to CAM physiology, the data presented here provide strong support for the long-held view that the ability to use CAM, and to use it increasingly in response to drought stress, provides a genuine adaptive advantage in terms of prolonging net atmospheric CO_2 fixation during drought progression (Figure 4D; Kluge and Fischer, 1967; Osmond, 1978). The wild type and line *rPPC1-A* achieved, respectively, net atmospheric CO_2 fixation of 18,568 and 19,071 μmol m^{-2} over the 22-d drought progression, whereas line *rPPC1-B* only achieved 13,983 μmol m^{-2} net atmospheric CO_2 fixation (Supplemental Table 4). Thus, the wild type, with its fully functional CAM system, was able to fix 33% more CO_2 over the entire drought treatment period than the mutant.

Insights into the Evolutionary Trajectory from C_3 to CAM

The discovery that the very low level of PPC activity in the *rPPC1-B* transgenic line was associated with nocturnal refixation of respiratory CO_2 revealed that even a small increase in PPC activity in the dark period may be sufficient to support a minimal, but functional, CAM cycle. Thus, during CAM evolution from ancestral C_3 species, small increases in nocturnal PPC activity in photosynthetic mesophyll cells behind closed stomata may have been sufficient to support the refixation of respiratory CO_2 to stored vacuolar malic acid, allowing its subsequent decarboxylation in

the light, leading to partial stomatal closure, enhanced WUE, and improved Rubisco carboxylation efficiency relative to the oxygenase (Edwards, 2019). However, despite our data for *Kalanchoë* supporting this evolutionary perspective on the progression to CAM, initial attempts to increase the expression of core CAM pathway enzymes in the C_3 model species Arabidopsis have not reciprocated the phenotype of even the most strongly silenced *rPPC1-B* line reported here. Constitutive overexpression of the CAM-specific *PPC* isogene from *M. crystallinum* in Arabidopsis led to increased stomatal conductance and titratable acidity (Lim et al., 2019). However, the increased stomatal conductance was measured in the middle of the light period, and the timing of the titratable acidity measurements relative to the light/dark cycle was not mentioned (Lim et al., 2019). Therefore, it is difficult to compare those results with the results presented here documenting alterations in nocturnal stomatal opening and atmospheric CO_2 fixation and dawn-phased malate accumulation in the *rPPC1* transgenic lines of *Kalanchoë*. It should be noted, however, that the *K. laxiflora* lines with reduced CAM-specific *PPC1* transcript levels still possessed succulent leaves with large mesophyll cells plus wild-type levels of key CAM transcripts and enzymes such as PPDK. Thus, the *rPPC1* plants were by no means directly comparable to the transgenic Arabidopsis lines reported by Lim et al. (2019).

Impact of *PPC1* Silencing on the CAM Circadian Rhythm of CO_2 Fixation

The circadian rhythm of CO_2 fixation observed for CAM species of *Kalanchoë* under constant free-running conditions is a classic example of a plant clock output rhythm driven by the underlying multi-gene-loop, autoregulatory core oscillator mechanism in the nucleus that sets the time (Hartwell, 2006). Under LL conditions, the CAM-associated circadian rhythm of CO_2 fixation dampened toward almost complete arrhythmia in detached leaves and whole, young plants of *rPPC1-B*, and CO_2 was fixed continuously (Figures 6A and 6B). The collapse of the CO_2 circadian rhythm suggests that CO_2 fixation by Rubisco in *rPPC1-B* was not subject to robust and high-amplitude circadian control, certainly not in comparison with the rhythm of atmospheric CO_2 fixation during CAM in the wild type (Figure 6B). In *K. daigremontiana*, Rubisco is thought to make a large contribution to the observed rhythm of CO_2 assimilation under LL conditions, as the level of malate does not oscillate (Wyka and Lüttge, 2003). By contrast, online carbon isotope discrimination measurements demonstrated that the LL CO_2 rhythm of CAM leaves of *M. crystallinum* had a Rubisco carbon isotope discrimination early in each subjective dark period, which then transitioned to a PPC carbon isotope ratio later in the subjective dark (Davies and Griffiths, 2012). In *rPPC1-B* (with no detectable PPC), the remaining Rubisco-mediated rhythm displayed, at best, only a very weak rhythm of CO_2 assimilation (Figure 6A). This suggests that C_3 carboxylation via Rubisco only makes a small contribution to the LL rhythm in *K. laxiflora* CAM leaves, or perhaps the robust, high amplitude CO_2 rhythm of the wild type depends on interplay between high PPC activity and Rubisco, which ceases in the absence of *PPC1*. Overall, the weakly rhythmic-to-arrhythmic pattern of CO_2 assimilation in *rPPC1-B* under LL was very similar to that of C_3 *M. crystallinum* (Davies and Griffiths, 2012).

Regulation of Core Clock Genes in *rPPC1-B*

Previous reports for other CAM species have emphasized that most core circadian clock genes share their pattern and phasing of diel transcript regulation between Arabidopsis and, for example, *Agave*, pineapple, and white stonecrop (*Sedum album*; Sharma et al., 2017; Yin et al., 2018; Wai et al., 2019). These reports therefore emphasize that the timing of core clock genes is conserved between widely divergent species, regardless of the underlying mechanism of photosynthetic CO_2 fixation, which is consistent with the ancestral role of the core circadian clock in the temporal control and optimization of many biological processes in plants. However, individual studies have identified specific core clock genes, or genes closely associated with the core clock, that were differentially expressed and/or temporally phased in certain CAM species relative to Arabidopsis. For example, RNA sequencing (RNA-seq)-based transcriptome analysis in *A. americana* identified a gene related to the clock-associated output pathway gene *RVE1* (Rawat et al., 2009), which was rescheduled to the dark period in *Agave* but peaked phased to dawn in Arabidopsis (Yin et al., 2018). The *K. laxiflora RVE1-like* gene measured here reached its 24-h transcript peak phased to dawn in LD cycles (Figure 5) and was repressed in *rPPC1-B* relative to the wild type. Under LL, *RVE1-like* was induced in *rPPC1-B* relative to the wild type, and its transcript abundance oscillated robustly, with a higher amplitude oscillation than the wild type (Figure 7). These findings suggest that the *RVE1-like* gene measured here does not likely share a role in the circadian coordination of the daily CAM cycle, as has been hypothesized for *Agave RVE1*. In fact, based on our current data for the *rPPC1* lines, it is possible that *RVE1-like* might function in coupling the core clock to the robust rhythm of DF observed in the *rPPC1* transgenic lines (Figure 6C).

In pineapple, the core clock genes *PRR5* and *PRR9* are rhythmic specifically in the green leaf tip tissue that performs CAM (Sharma et al., 2017). By contrast, the *PRR7*, *PRR3/7*, and *PRR9* transcripts measured in this study were rhythmic over the LD cycle in the wild type, *rPPC1-A*, and *rPPC1-B*, although the levels of all three *PRR* transcripts were higher in *rPPC1-B* relative to the wild type (Figure 5). However, the abundance and rhythmicity of *PRR3/7* and *PRR9* collapsed in *rPPC1-B* under LL conditions, whereas *PRR7* was induced and rhythmic (Figure 7). In *S. album*, a member of the Crassulaceae along with *Kalanchoë*, the induction of weak CAM cycling in response to drought stress led to the repression of transcripts related to *GI* and *FKF1* and the induction of transcripts related to *CCA1* and *TOC1* (Wai et al., 2019). However, the timing of peak transcript abundance for core clock gene orthologs was largely consistent between C_3 and CAM-cycling leaf samples of *S. album*, with phase delays of 2 to 4 h at most for *PRR1_A* and *PRR5_A*, *PRR5_B*, and *PRR5_D* (Wai et al., 2019). In *rPPC1-B* under LD cycles, only changes in the transcript peaks of *CCA1-2* (down), *TOC1-1* (up), and *TOC1-2* (up) were detected (Figure 5). The timing of the peaks and troughs of these transcripts remained the same between the wild type and both *rPPC1* lines. *GI* and *FKF1* transcript oscillations and peak abundance were remarkably similar between the wild type and the two *rPPC1* lines under LD

cycles (Figure 5). However, under LL conditions, *CCA1-2*, *TOC1-1*, *TOC1-2*, *GI*, and *FKF1* were all induced relative to the wild type and oscillated more robustly, with lengthening periods as the LL time course progressed (Figure 7). Overall, there were no clear and consistent correlations between the transcript abundance cycles of core clock gene transcripts reported here for *K. laxiflora* wild type and RNAi lines with reduced *PPC1* levels and the published RNA-seq data for the LD cycles of transcript abundance of the orthologous genes in *Agave*, pineapple, and *S. album*. Furthermore, it was not possible to detect any temporal patterns of regulation of core clock gene transcripts between different species or between C_3 and CAM tissues in individual species, which would suggest that conserved alterations in the core clock have accompanied the evolution of CAM in these diverse CAM lineages.

Contrasting Core Clock Responses between *rPPC1* and *rPPCK1* RNAi Lines

Similar to the LL CO_2 fixation phenotype reported here for *rPPC1-B*, transgenic *K. fedtschenkoi* lines lacking *PPCK1* also lost the CO_2 fixation rhythm, and the transcript oscillations of many core clock genes were altered (Boxall et al., 2017). However, different core clock genes were perturbed in *rPPC1-B* compared with those whose rhythmic regulation changed in the *rPPCK1* lines of *K. fedtschenkoi* (compare Boxall et al., 2017 with Figure 7). In *rPPC1-B*, *CCA1-1* transcript oscillations dampened, and both *TOC1-1* and *TOC1-2* transcripts were upregulated and oscillated with a delayed peak phase relative to the wild type (Figures 7H, 7J, and 7K). By contrast, in line *rPPCK1-3*, the transcription of clock genes *CCA1-1*, *CCA1-2*, and *TOC1-2* dampened rapidly toward arrhythmia under LL free-running conditions, whereas *TOC1-1* was upregulated and rhythmic (Boxall et al., 2017). Furthermore, while *PRR7* was upregulated and rhythmic in *rPPC1-B* (Figure 7), the same gene dampened to arrhythmia in *rPPCK1-3* after an initial induced peak during the first 6 h of LL (Boxall et al., 2017). The evening-phased genes *GI* and *FKF1* were induced and rhythmic under LL conditions in both *rPPC1-B* and *rPPCK1-3*, but the level of transcript induction and the rhythm amplitude were much greater in *rPPC1-B* (Figures 7U and 7V), suggesting that these two clock genes are more important for robust oscillations in C_3 leaves.

Overall, these differences between the rhythms of core clock genes in *rPPC1-B* and *rPPCK1-3* revealed that the clock responded very differently to the silencing of two interconnected genes that lie at the heart of the circadian control of nocturnal CO_2 fixation. Elucidating the mechanistic basis for these differences should be a fruitful avenue for further investigation, especially in light of the proposed crosstalk between CAM-associated metabolites and regulation within the core clock (Boxall et al., 2017), which was further supported by the clock gene phenotypes reported here (Figure 7).

Interactions between Sugars Linked to CAM and the Core Circadian Clock

In Arabidopsis, sugars associated with primary photosynthetic metabolism play a role in the entrainment of the core circadian oscillator in the nucleus (Haydon et al., 2013). In particular, *PRR7* is thought to be required for sensing metabolic status and coordinating the clock with photosynthesis (Haydon et al., 2013). In *rPPC1-B*, the low sucrose levels at 2 h after dawn (Figure 3C) may be sensed via a mechanism involving *PRR7* (Boxall et al., 2017). However, in *Kalanchoë*, a second *PRR7*-related gene, *PRR3/7*, produced the more abundant transcript and displayed a transcript peak 2 h before dusk under LD (Figure 5T). In the wild type, *PRR3/7* may function as part of a signal transduction pathway that senses metabolic status at dusk when primary CO_2 fixation begins (Haydon et al., 2013; Boxall et al., 2017).

rPPC1 and *rPPCK1* Mutants Display Contrasting Levels of DF Circadian Rhythms

DF circadian rhythms were more robust in the wild type than in *rPPC1-A* and *rPPC1-B* (Figure 6C). This result represents one of the most striking contrasts to the previous finding of arrhythmic DF in the *K. fedtschenkoi rPPCK1-3* line (Boxall et al., 2017). This fundamental difference provides important insights into the regulatory signal transduction network underpinning the DF rhythm, which originates from inside the chloroplasts due to the changing redox state of the plastoquinone pool (Gould et al., 2009). In terms of core clock gene regulation under both LD and LL, *CCA1-2*, *TOC1-2*, *PRR7*, and the clock-controlled gene *CDF2* were all induced and rhythmic in *rPPC1-B*. Thus, *CCA1-2*, *TOC1-2*, *PRR7*, and *CDF2* are the most likely candidates for driving the induction and robust LL rhythmicity of DF in *rPPC1-B*. Conversely, the decline in the amount and rhythmicity of these transcripts in *rPPCK1-3* may play a role in the dampening of the DF rhythms in the absence of nocturnal phosphorylation of PPC1 (Boxall et al., 2017).

These results also allow us to propose that robust rhythmicity of the CAM-associated CO_2 fixation rhythm in wild-type *Kalanchoë* is most likely driven by an underlying oscillator consisting of *CCA1-1*, *PRR3/7*, *PRR9*, and *LNK3-like*. This hypothesis is supported by the finding that the rhythmicity of these core clock components responded in the same way in both *rPPC1-B* and the previously reported *rPPCK1-3* transgenic lines of *Kalanchoë* (Boxall et al., 2017). However, only a limited set of core clock and clock-associated genes has been profiled under LL in *rPPC1-B* and *rPPCK1-3*, making it likely that other clock-associated genes are also involved in driving robust CAM CO_2 fixation rhythms and robust DF rhythms.

Perturbation of Diel Rhythms of Gene Transcript Oscillations in GCs

A key gap in the current understanding of the molecular genetics underpinning the physiology associated with CAM centers on the cell signaling mechanisms that mediate the inverse pattern, relative to C_3, of stomatal opening and closing (Borland et al., 2014; Males and Griffiths, 2017). The GCs of CAM leaves and stems are thought to respond directly to the internal supply of CO_2. This theory has recently led several groups to use whole-leaf RNA-seq data sets to investigate alterations, relative to C_3 leaves, in the temporal phasing of known GC regulatory genes and membrane transporters (Abraham et al., 2016; Wai and VanBuren, 2018; Yin

et al., 2018; Heyduk et al., 2019; Moseley et al., 2019). However, these studies did not use enriched GCs as the source of RNA, and therefore the data that were mined represented all leaf cell types, including palisade and spongy mesophyll, GCs, subsidiary cells, phloem, phloem companion cells, xylem, bundle sheath, and water storage parenchyma in *Agave* and pineapple. Thus, the rescheduling of the temporal patterns of candidate GC genes in these data sets may have been complicated by transcripts from the same genes that were functional in other leaf cell types.

Separated epidermal peels from *Kalanchoë* CAM leaves are enriched for intact GCs. We leveraged this feature in order to compare the temporal pattern of transcript regulation between GC-enriched epidermal peels of the wild type and *rPPC1-B* (Figure 8). Relative to the wild type, a wide range of genes known to be involved in stomatal opening and closing displayed alterations in transcript abundance and/or the timing of the daily transcript peak (Figures 8A to 8U). These results support the theory that the measured changes in transcript abundance and temporal patterns for a range of GC regulatory genes were connected to the measured changes in stomatal opening and closing (Figure 4B).

Thus, the upregulation of *HT1*, *SKOR*, and *MYB61* in the wild type relative to *rPPC1-B* and the downregulation of a wide range of genes in the wild type, including *SLAC1*, *PP2C*, *SOS2*, *ACA2*, *ECA4*, and *MYB60*, are likely important regulatory changes that facilitate nocturnal stomatal opening and light period closure (Figures 4 and 8). As *MYB60* is required for stomatal opening in response to light in C_3 Arabidopsis (Cominelli et al., 2005), it is particularly noteworthy that its transcript abundance in wild-type *K. laxiflora* GC-enriched epidermal peels peaked at dusk, when stomata open in the wild type (Figure 8S). Furthermore, in *rPPC1-B*, *MYB60* also had a dramatic threefold to fourfold induction at dawn relative to the wild type, suggesting that high *MYB60* transcript levels at the start of the light period may play a key role in the observed light period stomatal opening of the *rPPC1-B* line (Figure 4B). It was also notable that *rPPC1-B* continued to have a peak of *MYB60* transcripts phased to dusk, as observed for the wild type, which is in agreement with the observation that *rPPC1-B* did open its stomata slightly throughout the dark period (Figure 4B). However, this nocturnal stomatal opening was futile in terms of atmospheric CO_2 fixation, as *rPPC1-B* released respired CO_2 from its leaves throughout the dark period (Figure 4A). Overall, *MYB60*, as well as several other misregulated GC signaling, ion channel, and metabolite transporter genes (Figure 8; Supplemental Figure 5), represent key targets for future genetic manipulation experiments in transgenic *Kalanchoë* aimed at understanding the important regulators underpinning the inverse stomatal control associated with CAM.

Informing Biodesign Strategies for Engineering CAM into C_3 Crops

Efforts are underway to engineer CAM and its associated increased WUE into C_3 species as a means to develop more climate-resilient crop varieties that can continue to fix CO_2 and grow in the face of drought while using water more wisely than C_3 varieties (Borland et al., 2014, 2015; Lim et al., 2019). The data presented here for the *rPPC1* loss-of-function lines of *K. laxiflora* confirm experimentally the proposed core role of *PPC1* for efficient and optimized CAM. Our results also provide encouragement that the level of overexpression of a CAM-recruited *PPC1* gene introduced into an engineered C_3 species may not need to be as high as the level found in extant obligate CAM species, because reducing *PPC1* levels to only 43% of wild-type activity in line *rPPC1-A* led to plants that were still capable of full CAM and fixed more CO_2 than the wild type over 3 weeks of drought (Figure 4D).

The results presented here also emphasize that only certain subcomponents of the core circadian clock are essential for the temporal optimization of CAM in *Kalanchoë*, which in turn further simplifies the challenge of achieving correct temporal control of an engineered CAM pathway introduced into a C_3 species. It is clear from our current RT-qPCR data that the transgenic manipulation of the expression and regulation of *CCA1-1*, *PRR3/7*, *PRR9*, and *LNK3-like* in *Kalanchoë* using RNAi, overexpression, and/or CRISPR-Cas-mediated gene editing will allow the further refinement of the evolving model for the subset of core clock genes that form the transcription-translation feedback loop that underpins the temporal optimization of CAM. However, in addition, transcriptome-wide analysis of the light/dark regulation of all detectable transcripts in LP6 of *rPPC1-B* compared with the wild type will allow the identification of other candidate core clock genes that were not profiled in the targeted RT-qPCR analysis presented here.

METHODS

Plant Materials

Kalanchoë laxiflora plants were propagated clonally from adventitious plantlets in the leaf margin using the same clonal stock originally obtained from the Royal Botanic Gardens (RBG), Kew, in 2008 (accession number 1982-6028), which was kindly provided by the RBG-Kew Living Collection but misidentified under the name *Kalanchoë fedtschenkoi*. Plants were initially grown in a heated transgenic greenhouse with supplementary lighting (Gavita reflector lamps HPS-R Agro 600 W S-281), providing year-round 16 h of light/8 h of dark, minimum light intensity at plant height of 300 to 400 μmol photons m^{-2} s^{-1}, and a minimum temperature of 20°C. Prior to all experiments, clonal populations of developmentally synchronized plants raised under greenhouse conditions were entrained in a Snijders Microclima MC-1000 growth cabinet for 7 d under LD and/or subsequently released into LL conditions according to Boxall et al. (2017).

Time-Course Experiments

For both LD and LL time-course experiments, opposite pairs of LP6 were collected every 4 h over an LD cycle (12:12 LD), starting 2 h (02:00 h) after the lights came on at 00:00 h. Plants were entrained for 7 d in a Snijders Microclima MC-1000 growth cabinet with fluorescent lamps (20 Phillips TL5-HO and 3 Phillips TLD-90, providing a mixed spectrum from 400 to 650 nm) set to 12-h-light (450 μmol photons m^{-2} s^{-1}), 25°C, 60% humidity/12-h-dark, 15°C, 70% humidity conditions. For constant light, constant temperature, constant humidity (LL) free-running circadian time-course experiments, plants were entrained under LD conditions as above and switched to LL after a dark period. For LL, the constant conditions were as follows: light 100 μmol photons m^{-2} s^{-1}, temperature 15°C, and humidity 70%. For both LD and LL experiments, LP6 were sampled every 4 h from three individual (clonal) plants, starting at 02:00 h (2 h after lights-on). All leaf samples were immediately frozen in liquid nitrogen and stored at −80°C until use.

Generation of Transgenic *K. laxiflora* Lines

An intron-containing hairpin RNAi construct was designed to target the silencing of both copies of the CAM-associated *PPC1* gene in the tetraploid *K. laxiflora* genome (JGI Phytozome accession numbers Kalax.0018s0056.1 and Kalax.0021s0061.1, which are the *K. laxiflora* orthologs of the previously characterized *K. fedtschenkoi* CAM-associated *PPC1*, GenBank accession number KM078709). A 323-bp fragment was amplified from CAM leaf cDNA using high-fidelity PCR with KOD Hot Start DNA Polymerase (Merck). The amplified fragment spanned the 3′ end of the *PPC1* coding sequence and extended into the 3′ untranslated region to ensure specificity of the silencing to both of the aforementioned CAM-associated *PPC1* gene copies. Alignment of the 323-bp region with the homologous regions from the three other plant-type *PPC* genes, and their homeologs, in the *K. laxiflora* genome demonstrated that none of the other *PPC* genes shared any 21-nucleotide stretches that were an exact match for the 323-bp *PPC1* RNAi fragment. Thus, the RNAi construct in the hairpin RNA binary vector used to generate the stable transgenic lines was predicted to silence only the two homeologous copies of the CAM-associated *PPC1* and to be equally specific and efficient at silencing both copies. This specificity and equality of silencing efficiency was confirmed by the RT-qPCR data in Figure 1, as the qPCR primers targeted both copies of the CAM-associated *PPC1* (Supplemental Figure 1), and so the quantitative signal is representative of the averaged signal for the transcript abundance of the two gene copies.

The primers used for the amplification of the *PPC1* gene fragment cloned to generate the hairpin RNAi binary construct were *PPC1 RNAi F* (5′-CACCAAGCTACCAAGTGCCGGTG-3′) and *PPC1 RNAi R* (5′-CCC TCCTGCTGCTGCTGCTGC-3′). The PCR product was cloned into the pENTR/D Gateway-compatible entry vector, as described previously (Dever et al., 2015). Following confirmation of the correct sequence and orientation of the *PPC1* fragment in the ENTRY vector using Sanger sequencing, the pENTR/D *PPC1* RNAi clone was recombined into intron-containing hairpin RNAi binary vector pK7GWIWG2(II) (Karimi et al., 2002) using LR Clonase II enzyme mix (Life Technologies). *Agrobacterium tumefaciens*-mediated stable transformation of *K. laxiflora* was achieved using a method described previously for the very closely related species *K. fedtschenkoi* (Dever et al., 2015), with the following changes. For *K. laxiflora* transformation, the initial sterile leaf explants used for dipping in *A. tumefaciens* GV3101 carrying the engineered binary vector were generated by germinating surface-sterilized *K. laxiflora* seeds on Murashige and Skoog medium with Gamborg's B-5 vitamins (Murashige and Skoog, 1962; Gamborg et al., 1968) and 3% (w/v) Suc. Four- to 6-week-old seedlings grown by tissue culture were chopped into explants for transformation in a sterile laminar flow bench using a sterile scalpel. The explants were dipped in the *A. tumefaciens* suspension carrying the *PPC1* RNAi binary vector and then cocultivated and regenerated as previously described by Dever et al. (2015).

High-Throughput Leaf Acidity and Starch Content Screens

Leaf acidity (as a proxy for leaf malate content) and leaf starch content were screened in stained leaf discs using chlorophenol red and iodine solution at both dawn and dusk as described by Cushman et al. (2008). For each transgenic line, leaf discs were sampled from LP6 in triplicate at 1 h before dawn and 1 h before dusk and stained in a 96-well plate format.

Net CO_2-Exchange Measurement Using Whole Young Plants

Whole-plant gas-exchange measurements were collected over a period of 27 d using 2-month-old plants at the nine-leaf-pair stage (results shown in Figure 4D). Four individual clones per line were potted in 150-mL beakers of compost mix, which was initially watered to field capacity, and the beakers were sealed with Parafilm around the rim of the beaker and the base of the stem. Beakers with potted plants were lowered into the lower half of each of the 12 gas-exchange cuvettes. Lids were sealed over each plant using bulldog clips to create a gas-tight seal due to the compression of foam rubber that lined the joint between the lower and upper half of each gas-exchange cuvette. During the 27-d time period, the progression into drought of young, initially well-watered, wild-type plants was documented as they transitioned from displaying all four phases of CAM with a relatively low proportion of dark period CO_2 fixation in phase I on day 1, through to full CAM (only phase I dark CO_2 fixation and phase III CO_2 refixation behind closed stomata throughout the light) from day 12, followed by recovery of all four phases of CAM after rewatering on day 22. Measurements were made using a custom-built, 12-channel infrared gas analyzer system (PP Systems), which allowed for individual environmental control (CO_2/H_2O) and measurement of the rates of CO_2 uptake for each of 12 gas-exchange cuvettes, with measurements collected every ~18 min. The system was described in full by Dever et al. (2015) but was expanded here with the addition of six gas-exchange cuvettes, thereby doubling the scope for replication and throughput. The experiment was performed using four individual clonal young plants (2 months old, nine leaf pairs) per line: the wild type, *rPPC1-A*, and *rPPC1-B*. The fourfold replicated wild-type and *rPPC1* lines were compared in neighboring gas-exchange cuvettes during each experimental run, such that the data are directly comparable between each line. As the entire gas-exchange system was housed in a Snijders Microclima MC-1000 growth cabinet, all 12 gas-exchange cuvettes were under identical conditions in terms of light intensity and temperature.

Measurement of Circadian Rhythms of Net CO_2 Exchange under Constant Light and Temperature Free-Running Conditions

Various *Kalanchoë* species display a persistent and robust circadian rhythm of CO_2 exchange when detached CAM leaves are measured with their petiole in distilled water (Wilkins, 1959). This discovery led to the current understanding that the endogenous circadian clock underpins the optimized temporal control of CAM in *Kalanchoë* (Hartwell, 2006; Boxall et al., 2017). The circadian rhythm of CO_2 exchange was measured for the wild type, *rPPC1-A*, and *rPPC1-B* using both detached LP6 sampled from 4-month-old mature plants and intact young plants at the nine-leaf-pair stage (2 months old). The 12-cuvette gas-switching CIRAS-DC-based gas-exchange system (Dever et al., 2015) was used to measure both the detached LP6 and the intact young plants with their roots in compost mix. For detached LP6, leaves were detached from each line at the base of their petiole using a scalpel, and the cut petiole was immediately immersed in distilled water by pushing the petiole through a small hole cut in Parafilm covering a 150-mL beaker of distilled water. The gas-exchange cuvettes were designed to hold a 150-mL beaker in the lower half of the cuvette such that the leaves were enclosed in the clear, upside-down 1-liter beaker that formed the upper section of the cuvette in which gas exchange was measured. After the upper section of each cuvette was placed over the leaves or intact young plants, the upper and lower sections of the cuvettes were sealed using bulldog clips to clamp the join, which was coated in foam rubber sealing material to generate a gas-tight seal. To measure intact young plants, individual clones of each line at the nine-leaf-pair stage were potted in compost mix in 150-mL pots that fit into the base of the gas-exchange cuvettes, and Parafilm was used to seal around the upper rim of the beaker and the central stem of the young plant to prevent soil and root respiration from interfering with the gas exchange measured for the aboveground leaf pairs (LP1 to LP9). Plants were pre-entrained to LD cycles in a Snijders Microclima MC-1000 growth cabinet for 7 d as described above prior to release into LL free-running conditions at the end of the last dark period. For LL, the constant conditions were as follows: light 100 μmol photons m^{-2} s^{-1}, temperature 15°C, and humidity 70%. The entire gas-exchange system was housed inside a Snijders Microclima MC-1000 growth cabinet, so all 12 cuvettes were under identical conditions.

Measuring Net CO_2 Exchange in Attached LP6 Using the LI-6400XT System

The gas exchange of mature CAM leaves (LP6) was measured over a 12-h-light, 25°C, 60% humidity/12-h-dark, 15°C, 70% humidity cycle using an infrared gas analyzer (LI-6400XT, LI-COR) attached to a large CO_2 gas cylinder. Data were logged every 10 min using an autoprogram that tracked the light and temperature regimes of the growth cabinet.

Measuring Leaf Malate, Starch, and Sucrose Contents

LP6 (full CAM in the wild type) from mature plants were sampled into liquid nitrogen every 4 h and at dawn and dusk and stored at −80°C until use. Biological triplicates were sampled, where each replicate was a pair of leaves of the designated developmental age from a separate, developmentally synchronized, clonal plant of each line. The frozen leaf samples were prepared and assayed for malate and starch as described by Dever et al. (2015) using the published methods for assaying malate in an enzyme-linked spectrophotometric assay (Möllering, 1985) and starch (Smith and Zeeman, 2006). Sucrose, glucose, and fructose were assayed according to the manufacturer's protocol (Megazyme Technologies).

Chlorophyll Assays

Chlorophyll was assayed from mature greenhouse-grown plants from LP2 to LP7. Biological triplicates were sampled, where each replicate was a pair of leaves of the designated developmental age from a separate, developmentally synchronized, clonal plant of each line. Chlorophyll was extracted twice from 0.5-cm-diameter leaf discs in 2 mL of 80% (v/v) acetone and homogenized in a bead beater (PowerLyzer 24, Mo-Bio). The tubes were centrifuged at full speed in a benchtop microfuge at 4°C for 2 min, and the supernatants were combined and transferred to a new tube and protected from the light. Absorbance was read at 663 and 645 nm, and chlorophyll contents were calculated according to the published method (Arnon, 1949).

Total RNA Isolation and RT-qPCR

Leaf samples (LP6) for RNA isolation were collected from wild-type, *rPPC1-A*, and *rPPC1-B* plants every 4 h starting at 2 h after dawn for both 12-h-light/12-h-dark cycles and LL experiments. Biological triplicates were sampled, where each replicate was a pair of leaves of the designated developmental age from a separate, developmentally synchronized, clonal plant of each line. Total RNA was isolated from 100 mg of frozen, ground leaf tissue using an RNeasy kit (Qiagen) following the manufacturer's protocol with the addition of 13.5 μL of 50 mg mL^{-1} polyethylene glycol 20000 to 450 μL of RLC buffer used for each extraction. cDNA was synthesized from the total RNA using a Quantitect RT kit according to the manufacturer's instructions (Qiagen). The resulting cDNA was diluted 1:4 with molecular biology-grade water prior to use in RT-qPCR. Transcript levels were determined using a SensiFAST SYBR No Rox kit (Bioline) in an Agilent MX3005P qPCR System Cycler. The results for each target gene transcript of interest were normalized to the reference gene *THIOESTERASE/THIOL ESTER DEHYDRASE-ISOMERASE SUPERFAMILY PROTEIN* (Kalax.0134s0055.1 and Kalax.1110s0007.1; Arabidopsis [*Arabidopsis thaliana*] ortholog AT2G30720.1). Gene expression in a pool of RNA generated from LP6 samples collected every 4 h over an LD cycle was set to 1. Primers used for RT-qPCR analyses are listed in Supplemental Data Set 2 and were designed to target both homeologs of each gene present in the tetraploid genome. It should be noted that primers that were specific to both homeologs of *CCA1-1* did not target the two *CCA1-2* homeologs in the *K. laxiflora* genome. Likewise, the primers that we used to quantify transcripts from both homeologs of *TOC1-1* did not target the two *TOC1-2* homeologs.

Immunoblotting

Total protein extracts of *K. laxiflora* leaves were prepared according to Dever et al. (2015). One-dimensional SDS-PAGE and immunoblotting of leaf proteins were performed following standard methods. Blots were developed using the enhanced chemiluminescence system (GE Healthcare). Immunoblot analysis was performed using antisera to PPC raised against purified CAM leaf PPC from *Kalanchoë fedtschenkoi* (diluted 1:5000), kindly supplied by Hugh G. Nimmo, University of Glasgow (Nimmo et al., 1986), and the phosphorylated form of PPC (diluted 1:1000) raised against a phospho-PPC peptide from wheat (*Triticum aestivum*), kindly supplied by Cristina Echevarría, Universidad de Sevilla (González et al., 2002; Feria et al., 2008). The PPDK antibody (diluted 1:1000) was raised against maize (*Zea mays*) C_4 PPDK, and the phospho-PPDK antibody (diluted 1:3000) was raised against a synthetic phospho-peptide spanning the PPDK phosphorylation site in the maize C_4 PPDK. Both PPDK antibodies were kindly provided by Chris J. Chastain, Minnesota State University, Moorhead (Chastain et al., 2000, 2002). The specificity of the antibodies used and, in the case of the phospho-peptide-specific antibodies for PPC and PPDK, their target phospho-site amino acid sequences are described in the Supplemental Methods.

Growth Measurements

Mature plants of the wild type and the two *rPPC1* lines were grown from developmentally synchronized, clonal leaf plantlets in greenhouse conditions for 4 months. At the start of the drought treatment, all the plants were watered to full capacity. Water was withheld from at least six replicate plants of each line for 28 d, and at least six plants were maintained well-watered over the same period. The plants were harvested as separated aboveground (shoot) and belowground (root) tissues, weighed to determine fresh weight, and dried in an oven at 60°C until they reached a constant dry weight.

PPC Assays

LP6 samples were taken at 6 h into the light period and frozen in liquid nitrogen. Biological triplicates were sampled, where each replicate was LP6 from a separate, developmentally synchronized, clonal plant of each line. Frozen leaf tissue was ground in liquid nitrogen with a small quantity of acid-washed sand and the relevant enzyme-specific extraction buffer (~1 g of tissue to 3 mL of extraction buffer). Extracts were prepared and PPC assays were performed according to the extraction, desalting, and assay buffer conditions previously described by Dever et al. (2015).

Determination of the Apparent K_i of PPC for L-Malate in Rapidly Desalted Leaf Extracts

The apparent K_i of PPC for L-malate was determined using leaf extracts that were rapidly desalted as described by Carter et al. (1991). LP6 were collected at 10:00 h (2 h before the end of the 12-h-light period) and 18:00 h (middle of the 12-h-dark period) from three biological replicates of the wild type, *rPPC1-A*, and *rPPC1-B*. Each biological replicate was LP6 from a separate, developmentally synchronized, clonal plant of each line. The apparent K_i of PPC activity for feedback inhibition by L-malate was determined as described by Nimmo et al. (1984), with the modifications to the range of L-malate concentrations added to the assays as described by Boxall et al. (2017).

PPDK Assays

PPDK assays were performed using the extraction and assay buffers described previously (Kondo et al., 2000; Dever et al., 2015), with the addition of NADH and G6P (Salahas et al., 1990) and Cibercron Blue

(Burnell and Hatch, 1986). Biological triplicates were sampled, where each replicate was LP6 from a separate, developmentally synchronized, clonal plant of each line. Briefly, 0.3 g of powdered leaf tissue that had previously been ground to a fine powder in liquid nitrogen was extracted in 1 mL of ice-cold extraction buffer (containing 100 mM Tris, pH 8.0, 10 mM DTT, 1 mM EDTA, 1% [v/v] Triton, 2.5% [w/v] polyvinylpolypyrrolidone, 2% [w/v] polyethylene glycol 20000, 10 mM $MgCl_2$, 1 mM PMSF, 2 μM orthovanadate, and 10 μM Cibercron Blue) by grinding with a small quantity of acid-washed sand with a pestle and mortar. Extracts were vortexed for 30 s, and the pH was adjusted to pH 8.0. Extracts were then placed on ice for 10 min before spinning them at full speed in a benchtop microfuge at 4°C. The supernatant (500 μL) was desalted using PD minitrap Sephadex-G25 columns (GE Healthcare). The desalting buffer contained 100 mM Tris-HCl, pH 8.0, 10 mM $MgCl_2$, 10 mM DTT, 0.1 mM EDTA, and 10 μM Cibercron Blue. The desalted extracts were assayed in a plate reader at 340 nm using the following assay buffer: 100 mM Tris, pH 8.0, 5 mM DTT, 10 mM $MgCl_2$, 1.25 mM pyruvic acid, 2.5 mM $NaHCO_3$, 2.5 mM K_2HPO_4, 0.25 mM NADH, 2 units of malate dehydrogenase, and 6 mM G6P. The reactions were started by the addition of 0.2 units of PPC followed by 1.25 mM ATP (pH 8.0).

DF Measurements

The imaging system for DF was identical to the luciferase and DF imaging system previously described by Gould et al. (2009) with the exception of the CCD camera (Retiga LUMO CCD Camera, QImaging). DF was quantified using Imaris image-analysis software (Bitplane) to measure mean intensity for specific regions within each image. Background intensities were calculated for each image and subtracted to calculate a final DF value for each image (Gould et al., 2009).

DF Rhythm Analysis

K. laxiflora plants were grown in greenhouse conditions for 4 months and then entrained in 12-h-light (450 μmol m^{-2} s^{-1}), 25°C, 60% humidity/12-h-dark, 15°C, 70% humidity cycles in a Snijders Microclima MC-1000 growth cabinet for 7 d as previously described by Dever et al. (2015). At dawn on day 8, 1.5-cm leaf discs were punched from each LP6 for three biological replicates (i.e., 7 leaf discs from each biological replicate, totaling 21 leaf discs per line) and placed on 0.3% (w/v) Phytoagar (Duchefa Biochemie) on a 10-cm-square Petri dish. The Petri dish was left under 12-h-light, 25°C/12-h dark, 15°C cycles for a further 24 h to synchronize the leaf discs. At subjective dawn, the Petri dish was placed in the imaging system at 14°C in constant red-blue light (LL). DF images were collected every 1 h for 120 h as previously described by Gould et al. (2009) and Boxall et al. (2017). The DF images were processed as described by Gould et al. (2009). The luminescence was normalized by subtracting the Y value of the best straight line from the raw Y value. BioDare was used to carry out fast Fourier transform (nonlinear least squares) analysis and spectral resampling on each DF time-course series using the time window from 24 to 120 h in order to generate period estimates and calculate the associated RAE (Moore et al., 2014; Zielinski et al., 2014).

Accession Numbers

Sequence data associated with this article are available via the JGI Phytozome portal for the *K. laxiflora* genome: https://phytozome.jgi.doe.gov, *Kalanchoë laxiflora* v1.1. The specific gene identifiers for the genes measured in this work are provided in Supplemental Data Set 2.

Supplemental Data

Supplemental Figure 1. Loading control for immunoblot analyses and PPC malate sensitivity assays.

Supplemental Figure 2. Impact of loss of PPC activity on vegetative yield during growth under well-watered and drought-stressed conditions.

Supplemental Figure 3. Photographs demonstrating the visual appearance of small plants after 22 d drought prior to re-watering.

Supplemental Figure 4. Impact of leaf age on the development of the characteristic 24 h light/dark pattern of CAM-associated CO_2 exchange.

Supplemental Figure 5. Impact of the loss of PPC1 on the light/dark regulation of the transcript abundance of CAM-, starch-, and circadian clock-associated genes in the CAM leaf epidermis.

Supplemental Table 1. Student's *t* test analysis of PPC activity.

Supplemental Table 2. Student's *t* test analysis of PPDK activity.

Supplemental Table 3. Student's *t* tests for chlorophyll *a* and *b*.

Supplemental Table 4. Calculations for the cumulative total CO_2 fixation (area under the curve) by each line during the 27-day drought-stress and re-watering experiment.

Supplemental Data Set 1. Student's *t* test results for relative growth measurements between wild type (WT) and *rPPC1-B*.

Supplemental Data Set 2. Primers used for RT-qPCR.

Supplemental Methods. Specificity of qPCR primers and antibodies.

ACKNOWLEDGMENTS

We thank Hugh Nimmo (University of Glasgow), Cristina Echevarría (Universidad de Sevilla), and Chris Chastain (Minnesota State University) for providing the antibodies used in this study. This work was supported by the U.S. Department of Energy Office of Science, Genomic Science Program (grant DE-SC0008834) and in part by the Biotechnology and Biological Sciences Research Council (grant BB/F009313/1 to J.H.). The contents of this article are solely the responsibility of the authors and do not necessarily represent the official views of the DOE.

AUTHOR CONTRIBUTIONS

J.H. and S.F.B. designed the research; S.F.B. performed all of the experiments except some of the tissue culture work for the regeneration of the transgenic lines, which was performed by N.K., and the statistical analysis of the DF data, which was performed by P.J.D.G.; J.K. generated the RNAi binary construct for *PPC1*; L.V.D. performed the PPDK assays; J.L.W. grew and maintained the plants and helped with grinding and processing of leaf samples; P.J.D.G. helped S.F.B. with the DF experiments and the analysis and interpretation of the associated data; S.F.B. and J.H. wrote the article.

Received July 1, 2019; revised January 28, 2020; accepted February 9, 2020; published February 12, 2020.

REFERENCES

Abraham, P.E., et al. (2016). Transcript, protein and metabolite temporal dynamics in the CAM plant *Agave*. Nat. Plants **2:** 16178.

Ache, P., Becker, D., Ivashikina, N., Dietrich, P., Roelfsema, M.R.G., and Hedrich, R. (2000). GORK, a delayed outward

rectifier expressed in guard cells of *Arabidopsis thaliana*, is a K^+-selective, K^+-sensing ion channel. FEBS Lett. **486:** 93–98.

Alonso-Cantabrana, H., Cousins, A.B., Danila, F., Ryan, T., Sharwood, R.E., von Caemmerer, S., and Furbank, R.T. (2018). Diffusion of CO_2 across the mesophyll-bundle sheath cell interface in a C_4 plant with genetically reduced PEP carboxylase activity. Plant Physiol. **178:** 72–81.

Anderson, C.M., and Wilkins, M.B. (1989). Period and phase control by temperature in the circadian rhythm of carbon dioxide fixation in illuminated leaves of *Bryophyllum fedtschenkoi*. Planta **177:** 456–469.

Arnon, D.I. (1949). Copper enzymes in isolated chloroplasts: Polyphenol oxidase in *Beta vulgaris*. Plant Physiol. **24:** 1–15.

Blatt, M.R. (2016). Plant physiology: Redefining the enigma of metabolism in stomatal movement. Curr. Biol. **26:** R107–R109.

Boccalandro, H.E., Giordano, C.V., Ploschuk, E.L., Piccoli, P.N., Bottini, R., and Casal, J.J. (2012). Phototropins but not cryptochromes mediate the blue light-specific promotion of stomatal conductance, while both enhance photosynthesis and transpiration under full sunlight. Plant Physiol. **158:** 1475–1484.

Borland, A.M., Griffiths, H., Hartwell, J., and Smith, J.A.C. (2009). Exploiting the potential of plants with Crassulacean acid metabolism for bioenergy production on marginal lands. J. Exp. Bot. **60:** 2879–2896.

Borland, A.M., Guo, H.B., Yang, X., and Cushman, J.C. (2016). Orchestration of carbohydrate processing for Crassulacean acid metabolism. Curr. Opin. Plant Biol. **31:** 118–124.

Borland, A.M., Hartwell, J., Weston, D.J., Schlauch, K.A., Tschaplinski, T.J., Tuskan, G.A., Yang, X., and Cushman, J.C. (2014). Engineering Crassulacean acid metabolism to improve water-use efficiency. Trends Plant Sci. **19:** 327–338.

Borland, A.M., Wullschleger, S.D., Weston, D.J., Hartwell, J., Tuskan, G.A., Yang, X., and Cushman, J.C. (2015). Climate-resilient agroforestry: Physiological responses to climate change and engineering of Crassulacean acid metabolism (CAM) as a mitigation strategy. Plant Cell Environ. **38:** 1833–1849.

Boxall, S.F., Dever, L.V., Kneřová, J., Gould, P.D., and Hartwell, J. (2017). Phosphorylation of phospho*enol*pyruvate carboxylase is essential for maximal and sustained dark CO_2 fixation and core circadian clock operation in the obligate Crassulacean acid metabolism species *Kalanchoë fedtschenkoi*. Plant Cell **29:** 2519–2536.

Boxall, S.F., Foster, J.M., Bohnert, H.J., Cushman, J.C., Nimmo, H.G., and Hartwell, J. (2005). Conservation and divergence of circadian clock operation in a stress-inducible Crassulacean acid metabolism species reveals clock compensation against stress. Plant Physiol. **137:** 969–982.

Brilhaus, D., Bräutigam, A., Mettler-Altmann, T., Winter, K., and Weber, A.P.M. (2016). Reversible burst of transcriptional changes during induction of Crassulacean acid metabolism in *Talinum triangulare*. Plant Physiol. **170:** 102–122.

Burnell, J.N., and Hatch, M.D. (1986). Activation and inactivation of an enzyme catalyzed by a single, bifunctional protein: A new example and why. Arch. Biochem. Biophys. **245:** 297–304.

Cai, J., et al. (2015) The genome sequence of the orchid *Phalaenopsis equestris*. Nat. Genet. **47:** 65–72.

Carter, P.J., Nimmo, H.G., Fewson, C.A., and Wilkins, M.B. (1990). *Bryophyllum fedtschenkoi* protein phosphatase type 2A can dephosphorylate phosphoenolpyruvate carboxylase. FEBS Lett. **263:** 233–236.

Carter, P.J., Nimmo, H.G., Fewson, C.A., and Wilkins, M.B. (1991). Circadian rhythms in the activity of a plant protein kinase. EMBO J. **10:** 2063–2068.

Chastain, C.J., Botschner, M., Harrington, G.E., Thompson, B.J., Mills, S.E., Sarath, G., and Chollet, R. (2000). Further analysis of maize C_4 pyruvate,orthophosphate dikinase phosphorylation by its bifunctional regulatory protein using selective substitutions of the regulatory Thr-456 and catalytic His-458 residues. Arch. Biochem. Biophys. **375:** 165–170.

Chastain, C.J., Fries, J.P., Vogel, J.A., Randklev, C.L., Vossen, A.P., Dittmer, S.K., Watkins, E.E., Fiedler, L.J., Wacker, S.A., Meinhover, K.C., Sarath, G., and Chollet, R. (2002). Pyruvate,orthophosphate dikinase in leaves and chloroplasts of C_3 plants undergoes light-/dark-induced reversible phosphorylation. Plant Physiol. **128:** 1368–1378.

Chater, C., et al. (2015). Elevated CO_2-induced responses in stomata require ABA and ABA signaling. Curr. Biol. **25:** 2709–2716.

Cheng, N.-H., Pittman, J.K., Zhu, J.-K., and Hirschi, K.D. (2004). The protein kinase SOS2 activates the *Arabidopsis* H^+/Ca^{2+} antiporter CAX1 to integrate calcium transport and salt tolerance. J. Biol. Chem. **279:** 2922–2926.

Chollet, R., Vidal, J., and O'Leary, M.H. (1996). Phosphoenolpyruvate carboxylase: A ubiquitous, highly regulated enzyme in plants. Annu. Rev. Plant Physiol. Plant Mol. Biol. **47:** 273–298.

Cominelli, E., Galbiati, M., Vavasseur, A., Conti, L., Sala, T., Vuylsteke, M., Leonhardt, N., Dellaporta, S.L., and Tonelli, C. (2005). A guard-cell-specific MYB transcription factor regulates stomatal movements and plant drought tolerance. Curr. Biol. **15:** 1196–1200.

Cushman, J.C., Agarie, S., Albion, R.L., Elliot, S.M., Taybi, T., and Borland, A.M. (2008). Isolation and characterization of mutants of common ice plant deficient in Crassulacean acid metabolism. Plant Physiol. **147:** 228–238.

Cushman, J.C., Davis, S.C., Yang, X., and Borland, A.M. (2015). Development and use of bioenergy feedstocks for semi-arid and arid lands. J. Exp. Bot. **66:** 4177–4193.

Daloso, D.M., Williams, T.C.R., Antunes, W.C., Pinheiro, D.P., Müller, C., Loureiro, M.E., and Fernie, A.R. (2016). Guard cell-specific upregulation of sucrose synthase 3 reveals that the role of sucrose in stomatal function is primarily energetic. New Phytol. **209:** 1470–1483.

Daszkowska-Golec, A., and Szarejko, I. (2013). Open or close the gate: Stomata action under the control of phytohormones in drought stress conditions. Front. Plant Sci. **4:** 138.

Davies, B.N., and Griffiths, H. (2012). Competing carboxylases: Circadian and metabolic regulation of Rubisco in C3 and CAM *Mesembryanthemum crystallinum* L. Plant Cell Environ. **35:** 1211–1220.

DePaoli, H.C., Borland, A.M., Tuskan, G.A., Cushman, J.C., and Yang, X. (2014). Synthetic biology as it relates to CAM photosynthesis: Challenges and opportunities. J. Exp. Bot. **65:** 3381–3393.

Dever, L.V., Blackwell, R.D., Fullwood, N.J., Lacuesta, M., Leegood, R.C., Onek, L.A., Pearson, M., and Lea, P.J. (1995). The isolation and characterization of mutants of the C_4 photosynthetic pathway. J. Exp. Bot. **46:** 1363–1376.

Dever, L.V., Boxall, S.F., Kneřová, J., and Hartwell, J. (2015). Transgenic perturbation of the decarboxylation phase of Crassulacean acid metabolism alters physiology and metabolism but has only a small effect on growth. Plant Physiol. **167:** 44–59.

Edwards, E.J. (2019). Evolutionary trajectories, accessibility and other metaphors: The case of C4 and CAM photosynthesis. New Phytol **223:** 1742–1755.

Feria, A.B., Alvarez, R., Cochereau, L., Vidal, J., García-Mauriño, S., and Echevarría, C. (2008). Regulation of phospho*enol*pyruvate carboxylase phosphorylation by metabolites and abscisic acid during the development and germination of barley seeds. Plant Physiol. **148:** 761–774.

Fulton, D.C., et al. (2008). β-AMYLASE4, a noncatalytic protein required for starch breakdown, acts upstream of three active β-amylases in *Arabidopsis* chloroplasts. Plant Cell **20:** 1040–1058.

Gamborg, O.L., Miller, R.A., and Ojima, K. (1968). Nutrient requirements of suspension cultures of soybean root cells. Exp. Cell Res. **50:** 151–158.

Gaymard, F., Pilot, G., Lacombe, B., Bouchez, D., Bruneau, D., Boucherez, J., Michaux-Ferrière, N., Thibaud, J.B., and Sentenac, H. (1998). Identification and disruption of a plant shaker-like outward channel involved in K^+ release into the xylem sap. Cell **94:** 647–655.

González, M.-C., Echevarria, C., Vidal, J., and Cejudo, F.J. (2002). Isolation and characterisation of a wheat phosphoenolpyruvate carboxylase gene: Modelling of the encoded protein. Plant Sci. **162:** 233–238.

Gould, P.D., Diaz, P., Hogben, C., Kusakina, J., Salem, R., Hartwell, J., and Hall, A. (2009). Delayed fluorescence as a universal tool for the measurement of circadian rhythms in higher plants. Plant J. **58:** 893–901.

Grondin, A., Rodrigues, O., Verdoucq, L., Merlot, S., Leonhardt, N., and Maurel, C. (2015). Aquaporins contribute to ABA-triggered stomatal closure through OST1-mediated phosphorylation. Plant Cell **27:** 1945–1954.

Gross, S.M., Martin, J.A., Simpson, J., Abraham-Juarez, M.J., Wang, Z., and Visel, A. (2013). De novo transcriptome assembly of drought tolerant CAM plants, Agave deserti and Agave tequilana. BMC Genomics **14:** 563.

Hartwell, J. (2005). The co-ordination of central plant metabolism by the circadian clock. Biochem. Soc. Trans. **33:** 945–948.

Hartwell, J. (2006). The circadian clock in CAM plants. In Endogenous Plant Rhythms, A.J.W. Hall, and and H.G. McWatters, eds (Oxford, UK: Blackwell Publishing), pp. 211–236.

Hartwell, J., Dever, L.V., and Boxall, S.F. (2016). Emerging model systems for functional genomics analysis of Crassulacean acid metabolism. Curr. Opin. Plant Biol. **31:** 100–108.

Hartwell, J., Gill, A., Nimmo, G.A., Wilkins, M.B., Jenkins, G.I., and Nimmo, H.G. (1999). Phosphoenolpyruvate carboxylase kinase is a novel protein kinase regulated at the level of expression. Plant J. **20:** 333–342.

Hartwell, J., Smith, L., Wilkins, M., Jenkins, G., and Nimmo, H. (1996). Higher plant phosphoenolpyruvate carboxylase kinase is regulated at the level of translatable mRNA in response to light or a circadian rhythm. Plant J. **10:** 1071–1078.

Hashimoto, M., Negi, J., Young, J., Israelsson, M., Schroeder, J.I., and Iba, K. (2006). *Arabidopsis* HT1 kinase controls stomatal movements in response to CO_2. Nat. Cell Biol. **8:** 391–397.

Hashimoto-Sugimoto, M., Higaki, T., Yaeno, T., Nagami, A., Irie, M., Fujimi, M., Miyamoto, M., Akita, K., Negi, J., Shirasu, K., Hasezawa, S., and Iba, K. (2013). A Munc13-like protein in *Arabidopsis* mediates H^+-ATPase translocation that is essential for stomatal responses. Nat. Commun. **4:** 2215.

Haydon, M.J., Mielczarek, O., Robertson, F.C., Hubbard, K.E., and Webb, A.A.R. (2013). Photosynthetic entrainment of the *Arabidopsis thaliana* circadian clock. Nature **502:** 689–692.

Hedrich, R., and Geiger, D. (2017). Biology of SLAC1-type anion channels: From nutrient uptake to stomatal closure. New Phytol. **216:** 46–61.

Helfer, A., Nusinow, D.A., Chow, B.Y., Gehrke, A.R., Bulyk, M.L., and Kay, S.A. (2011). LUX ARRHYTHMO encodes a nighttime repressor of circadian gene expression in the *Arabidopsis* core clock. Curr. Biol. **21:** 126–133.

Heyduk, K., Hwang, M., Albert, V., Silvera, K., Lan, T., Farr, K., Chang, T.H., Chan, M.T., Winter, K., and Leebens-Mack, J. (2019). Altered gene regulatory networks are associated with the transition from C_3 to Crassulacean acid metabolism in *Erycina* (Oncidiinae: Orchidaceae). Front. Plant Sci. **9:** 2000.

Heyduk, K., Ray, J.N., Ayyampalayam, S., and Leebens-Mack, J. (2018). Shifts in gene expression profiles are associated with weak and strong Crassulacean acid metabolism. Am. J. Bot. **105:** 587–601.

Hiyama, A., Takemiya, A., Munemasa, S., Okuma, E., Sugiyama, N., Tada, Y., Murata, Y., and Shimazaki, K.I. (2017). Blue light and CO_2 signals converge to regulate light-induced stomatal opening. Nat. Commun. **8:** 1284.

Holtum, J.A.M., Hancock, L.P., Edwards, E.J., and Winter, K. (2017). Facultative CAM photosynthesis (Crassulacean acid metabolism) in four species of *Calandrinia*, ephemeral succulents of arid Australia. Photosynth. Res. **134:** 17–25.

Horrer, D., Flütsch, S., Pazmino, D., Matthews, J.S.A., Thalmann, M., Nigro, A., Leonhardt, N., Lawson, T., and Santelia, D. (2016). Blue light induces a distinct starch degradation pathway in guard cells for stomatal opening. Curr. Biol. **26:** 362–370.

Hu, H., Boisson-Dernier, A., Israelsson-Nordström, M., Böhmer, M., Xue, S., Ries, A., Godoski, J., Kuhn, J.M., and Schroeder, J.I. (2010). Carbonic anhydrases are upstream regulators of CO_2-controlled stomatal movements in guard cells. Nat. Cell Biol. **12:** 87–93.

Imes, D., Mumm, P., Böhm, J., Al-Rasheid, K.A., Marten, I., Geiger, D., and Hedrich, R. (2013). Open stomata 1 (OST1) kinase controls R-type anion channel QUAC1 in *Arabidopsis* guard cells. Plant J. **74:** 372–382.

Jezek, M., and Blatt, M.R. (2017). The membrane transport system of the guard cell and its integration for stomatal dynamics. Plant Physiol. **174:** 487–519.

Karimi, M., Inzé, D., and Depicker, A. (2002). GATEWAY vectors for Agrobacterium-mediated plant transformation. Trends Plant Sci. **7:** 193–195.

Kim, T.-H., Böhmer, M., Hu, H., Nishimura, N., and Schroeder, J.I. (2010). Guard cell signal transduction network: Advances in understanding abscisic acid, CO_2, and Ca^{2+} signaling. Annu. Rev. Plant Biol. **61:** 561–591.

Kinoshita, T., Doi, M., Suetsugu, N., Kagawa, T., Wada, M., and Shimazaki, K. (2001). Phot1 and phot2 mediate blue light regulation of stomatal opening. Nature **414:** 656–660.

Kluge, M., and Fischer, K. (1967). Relations between CO_2-exchange and transpiration in *Bryophyllum daigremontianum*. Planta **77:** 212–223.

Kondo, A., Nose, A., Yuasa, H., and Ueno, O. (2000). Species variation in the intracellular localization of pyruvate, Pi dikinase in leaves of Crassulacean-acid-metabolism plants: An immunogold electron-microscope study. Planta **210:** 611–621.

Kore-eda, S., Noake, C., Ohishi, M., Ohnishi, J., and Cushman, J.C. (2005). Transcriptional profiles of organellar metabolite transporters during induction of Crassulacean acid metabolism in *Mesembryanthemum crystallinum*. Funct. Plant Biol. **32:** 451–466.

Kore-eda, S., Nozawa, A., Okada, Y., Takashi, K., Azad, M.A., Ohnishi, J., Nishiyama, Y., and Tozawa, Y. (2013). Characterization of the plastidic phosphate translocators in the inducible Crassulacean acid metabolism plant *Mesembryanthemum crystallinum*. Biosci. Biotechnol. Biochem. **77:** 1511–1516.

Lee, S.B., Kim, H.U., and Suh, M.C. (2016). MYB94 and MYB96 additively activate cuticular wax biosynthesis in *Arabidopsis*. Plant Cell Physiol. **57:** 2300–2311.

Liang, Y.K., Dubos, C., Dodd, I.C., Holroyd, G.H., Hetherington, A.M., and Campbell, M.M. (2005). AtMYB61, an R2R3-MYB transcription factor controlling stomatal aperture in *Arabidopsis thaliana*. Curr. Biol. **15:** 1201–1206.

Lim, S.D., Lee, S., Choi, W.-G., Yim, W.C., and Cushman, J.C. (2019). Laying the foundation for Crassulacean acid metabolism (CAM) biodesign: Expression of the C_4 metabolism cycle genes of CAM in *Arabidopsis*. Front. Plant Sci. **10:** 101.

Liu, J., Ishitani, M., Halfter, U., Kim, C.S., and Zhu, J.K. (2000). The *Arabidopsis thaliana* SOS2 gene encodes a protein kinase that is required for salt tolerance. Proc. Natl. Acad. Sci. USA **97:** 3730–3734.

Lüttge, U., and Ball, E. (1978). Free running oscillations of transpiration and CO_2 exchange in CAM plants without a concomitant rhythm of malate levels. Z. Pflanzenphysiol. **90:** 69–77.

Ma, Y., Szostkiewicz, I., Korte, A., Moes, D., Yang, Y., Christmann, A., and Grill, E. (2009). Regulators of PP2C phosphatase activity function as abscisic acid sensors. Science **324:** 1064–1068.

Males, J., and Griffiths, H. (2017). Stomatal biology of CAM plants. Plant Physiol. **174:** 550–560.

Ming, R., et al. (2015). The pineapple genome and the evolution of CAM photosynthesis. Nat. Genet. **47:** 1435–1442.

Möllering, H. (1985). L-malate: Determination with malate dehydrogenase and aspartate aminotransferase. In Methods in Enzymatic Analysis, H.U. Bermeyer, J. Bermeyer, and and M. Grasstl, eds (Weinheim, Germany: Verlag Chemie), pp. 39–47.

Monroe, J.D., and Storm, A.R. (2018). The Arabidopsis β-amylase (BAM) gene family: Diversity of form and function. Plant Sci. **276:** 163–170.

Moore, A., Zielinski, T., and Millar, A.J. (2014). Online period estimation and determination of rhythmicity in circadian data, using the BioDare data infrastructure. In Plant Circadian Networks: Methods and Protocols, D. Staiger, ed (New York: Springer Science and Business Media), pp. 13–44.

Moseley, R.C., Tuskan, G.A., and Yang, X. (2019). Comparative genomics analysis provides new insight into molecular basis of stomatal movement in *Kalanchoë fedtschenkoi*. Front. Plant Sci. **10:** 292.

Murashige, T., and Skoog, F. (1962). A revised medium for rapid growth and bio-assays with tobacco tissue cultures. Physiol. Plant. **15:** 473–497.

Neuhaus, H.E., and Schulte, N. (1996). Starch degradation in chloroplasts isolated from C_3 or CAM (Crassulacean acid metabolism)-induced *Mesembryanthemum crystallinum* L. Biochem. J. **318:** 945–953.

Nimmo, G.A., Nimmo, H.G., Fewson, C.A., and Wilkins, M.B. (1984). Diurnal changes in the properties of phosphoenolpyruvate carboxylase in *Bryophyllum* leaves: A possible covalent modification. FEBS Lett. **178:** 199–203.

Nimmo, G.A., Nimmo, H.G., Hamilton, I.D., Fewson, C.A., and Wilkins, M.B. (1986). Purification of the phosphorylated night form and dephosphorylated day form of phosphoenolpyruvate carboxylase from *Bryophyllum fedtschenkoi*. Biochem. J. **239:** 213–220.

O'Leary, B., Park, J., and Plaxton, W.C. (2011). The remarkable diversity of plant PEPC (phosphoenolpyruvate carboxylase): Recent insights into the physiological functions and post-translational controls of non-photosynthetic PEPCs. Biochem. J. **436:** 15–34.

Osmond, C.B. (1978). Crassulacean acid metabolism: A curiosity in context. Annu. Rev. Plant Physiol. Plant Mol. Biol. **29:** 379–414.

Park, S.Y., et al. (2009). Abscisic acid inhibits type 2C protein phosphatases via the PYR/PYL family of START proteins. Science **324:** 1068–1071.

Prasch, C.M., Ott, K.V., Bauer, H., Ache, P., Hedrich, R., and Sonnewald, U. (2015). β-Amylase1 mutant Arabidopsis plants show improved drought tolerance due to reduced starch breakdown in guard cells. J. Exp. Bot. **66:** 6059–6067.

Rawat, R., Schwartz, J., Jones, M.A., Sairanen, I., Cheng, Y., Andersson, C.R., Zhao, Y., Ljung, K., and Harmer, S.L. (2009). REVEILLE1, a Myb-like transcription factor, integrates the circadian clock and auxin pathways. Proc. Natl. Acad. Sci. USA **106:** 16883–16888.

Ritte, G., Heydenreich, M., Mahlow, S., Haebel, S., Kötting, O., and Steup, M. (2006). Phosphorylation of C6- and C3-positions of glucosyl residues in starch is catalysed by distinct dikinases. FEBS Lett. **580:** 4872–4876.

Salahas, G., Manetas, Y., and Gavalas, N.A. (1990). Assaying for pyruvate, orthophosphate dikinase activity: Necessary precautions with phosphoenolpyruvate carboxylase as coupling enzyme. Photosynth. Res. **24:** 183–188.

Santelia, D., and Lunn, J.E. (2017). Transitory starch metabolism in guard cells: Unique features for a unique function. Plant Physiol. **174:** 539–549.

Santiago, J., Dupeux, F., Round, A., Antoni, R., Park, S.-Y., Jamin, M., Cutler, S.R., Rodriguez, P.L., and Márquez, J.A. (2009). The abscisic acid receptor PYR1 in complex with abscisic acid. Nature **462:** 665–668.

Schluepmann, H., Pellny, T., van Dijken, A., Smeekens, S., and Paul, M. (2003). Trehalose 6-phosphate is indispensable for carbohydrate utilization and growth in *Arabidopsis thaliana*. Proc. Natl. Acad. Sci. USA **100:** 6849–6854.

Seo, P.J., Lee, S.B., Suh, M.C., Park, M.J., Go, Y.S., and Park, C.M. (2011). The MYB96 transcription factor regulates cuticular wax biosynthesis under drought conditions in *Arabidopsis*. Plant Cell **23:** 1138–1152.

Sharma, A., Wai, C.M., Ming, R., and Yu, Q. (2017). Diurnal cycling transcription factors of pineapple revealed by genome-wide annotation and global transcriptomic analysis. Genome Biol. Evol. **9:** 2170–2190.

Shi, J., Yi, K., Liu, Y., Xie, L., Zhou, Z., Chen, Y., Hu, Z., Zheng, T., Liu, R., Chen, Y., and Chen, J. (2015). Phospho*enol*pyruvate carboxylase in Arabidopsis leaves plays a crucial role in carbon and nitrogen metabolism. Plant Physiol. **167:** 671–681.

Smith, A.M., and Zeeman, S.C. (2006). Quantification of starch in plant tissues. Nat. Protoc. **1:** 1342–1345.

Smith, A.M., Zeeman, S.C., and Smith, S.M. (2005). Starch degradation. Annu. Rev. Plant Biol. **56:** 73–98.

Somers, D.E., Devlin, P.F., and Kay, S.A. (1998). Phytochromes and cryptochromes in the entrainment of the *Arabidopsis* circadian clock. Science **282:** 1488–1490.

Taybi, T., Patil, S., Chollet, R., and Cushman, J.C. (2000). A minimal serine/threonine protein kinase circadianly regulates phospho*enol*pyruvate carboxylase activity in Crassulacean acid metabolism-induced leaves of the common ice plant. Plant Physiol. **123:** 1471–1482.

Valerio, C., Costa, A., Marri, L., Issakidis-Bourguet, E., Pupillo, P., Trost, P., and Sparla, F. (2011). Thioredoxin-regulated β-amylase (BAM1) triggers diurnal starch degradation in guard cells, and in mesophyll cells under osmotic stress. J. Exp. Bot. **62:** 545–555.

von Caemmerer, S., and Furbank, R.T. (2003). The C_4 pathway: An efficient CO_2 pump. Photosynth. Res. **77:** 191–207.

von Caemmerer, S., and Griffiths, H. (2009). Stomatal responses to CO_2 during a diel Crassulacean acid metabolism cycle in *Kalanchoe daigremontiana* and *Kalanchoe pinnata*. Plant Cell Environ. **32:** 567–576.

Wai, C.M., and VanBuren, R. (2018). Circadian regulation of pineapple CAM photosynthesis. In Genetics and Genomics of Pineapple, R. Ming, ed (Cham, Switzerland: Springer International Publishing), pp. 247–258.

Wai, C.M., Weise, S.E., Ozersky, P., Mockler, T.C., Michael, T.P., and VanBuren, R. (2019). Time of day and network reprogramming

during drought induced CAM photosynthesis in *Sedum album*. PLoS Genet. **15:** e1008209.

Wild, B., Wanek, W., Postl, W., and Richter, A. (2010). Contribution of carbon fixed by Rubisco and PEPC to phloem export in the Crassulacean acid metabolism plant *Kalanchoe daigremontiana*. J. Exp. Bot. **61:** 1375–1383.

Wilkins, M.B. (1959). An endogenous rhythm in the rate of carbon dioxide output of *Bryophyllum*. I. Some preliminary experiments. J. Exp. Bot. **10:** 377–390.

Wilkins, M.B. (1992). Circadian rhythms: Their origin and control. New Phytol. **121:** 347–375.

Winter, K. (2019). Ecophysiology of constitutive and facultative CAM photosynthesis. J. Exp. Bot. **70:** 6495–6508.

Winter, K., and Holtum, J.A. (2014). Facultative Crassulacean acid metabolism (CAM) plants: Powerful tools for unravelling the functional elements of CAM photosynthesis. J. Exp. Bot. **65:** 3425–3441.

Wyka, T.P., and Lüttge, U.E. (2003). Contribution of C_3 carboxylation to the circadian rhythm of carbon dioxide uptake in a Crassulacean acid metabolism plant *Kalanchoë daigremontiana*. J. Exp. Bot. **54:** 1471–1479.

Yang, X., et al. (2017). The Kalanchoë genome provides insights into convergent evolution and building blocks of Crassulacean acid metabolism. Nat. Commun. **8:** 1899.

Yin, H., et al. (2018). Diel rewiring and positive selection of ancient plant proteins enabled evolution of CAM photosynthesis in *Agave*. BMC Genomics **19:** 588.

Yoshida, T., Anjos, L.D., Medeiros, D.B., Araújo, W.L., Fernie, A.R., and Daloso, D.M. (2019). Insights into ABA-mediated regulation of guard cell primary metabolism revealed by systems biology approaches. Prog. Biophys. Mol. Biol. **146:** 37–49.

Zhang, J., De-Oliveira-Ceciliato, P., Takahashi, Y., Schulze, S., Dubeaux, G., Hauser, F., Azoulay-Shemer, T., Tõldsepp, K., Kollist, H., Rappel, W.J., and Schroeder, J.I. (2018). Insights into the molecular mechanisms of CO_2-mediated regulation of stomatal movements. Curr. Biol. **28:** R1356–R1363.

Zhou, Y.P., Duan, J., Fujibe, T., Yamamoto, K.T., and Tian, C.E. (2012). AtIQM1, a novel calmodulin-binding protein, is involved in stomatal movement in *Arabidopsis*. Plant Mol. Biol. **79:** 333–346.

Zielinski, T., Moore, A.M., Troup, E., Halliday, K.J., and Millar, A.J. (2014). Strengths and limitations of period estimation methods for circadian data. PLoS One **9:** e96462.